Atomic Excitation Caused by α-Decay of the Nucleus

Atomic Excitation Caused by α-Decay of the Nucleus

By

Ian G. Breukelaar, M.A.Sc., B.A.Sc., B.Sc.

A Thesis

Submitted to the School of Graduate Studies

in Partial Fulfilment of the Requirements

for the Degree

Master of Science

McMaster University

MASTER OF SCIENCE (2006) McMaster University

(Physics and Astronomy) Hamilton, Ontario

TITLE: Atomic Excitation Caused by α-Decay of the Nucleus

AUTHOR: Ian Breukelaar, M.A.Sc., B.A.Sc., B.Sc.

SUPERVISOR: W. van Dijk, Y. Nogami

NUMBER OF PAGES: viii, 64

Abstract

The prevailing theory of Migdal for predicting the excitation probabilities of an atom from α-decay of the nucleus, considers the α-particle, after it has been emitted by the nucleus, as following a classical trajectory and interacting with the atom quantum mechanically. Recently an attempt was made to properly model this quantum mechanical phenomenon, in one dimension, with a quantum wavefunction treatment of the decaying α-particle, but a discrepancy was found between the new predictions and that of the traditional method. In light of this discrepancy, we have studied the various approximations made in that work. Our results concur with recent follow up work suggesting that agreement should be found between a fully quantum mechanical model and with the classical model of α-particle propagation where the α-particle is treated as a point particle.

Acknowledgements

I would first like to thank my supervisory committee for introducing me to this very interesting topic and for giving me the freedom to pursue various curiosities along the way. Specifically I would like to thank Professor Wytse van Dijk for his valuable role as a mentor and his example of what is involved with being a researcher. I would like to thank Professor Yukihisa Nogami for his tireless work and for reminding me of the power of the pencil. Too often in this modern day of computers we forget how insightful looking at a problem analytically can be. Thanks also to Professor Donald Sprung for sharing with me the finer points of quantum mechanics.

Thank you to the McMaster physics community as a whole. It is an exciting and stimulating research environment that I was fortunate to be a part of.

Finally, I would like to thank my beautiful wife for her continual support and limitless patience with my never ending preoccupation with physics. Muchas gracias.

Table of Contents

List of Figures

Chapter 1

Introduction

The state of scientific knowledge has developed to the point where very accurate theories are in place to explain the very small and the very large. In every day life though, we rely on classical physics for such things as the physics of baseball or the scattering of billiard balls. It may then come as a surprise that classical physics is still used in predicting atomic excitations due to α-decay of a nucleus. This is an inherently quantum mechanical and time-dependent phenomenon whereby an α-particle leaks or tunnels out of a nucleus, and between leaving the nucleus and leaving the atom, has a probability of interacting with the atomic electrons and exciting them to higher energy levels. The half life for decay may, in some cases, be long, with much of the α-particle wavefunction remaining within the nucleus, long after the tunnelling process begins. However, the prevailing theory by Migdal (Migdal 1941), dating back to the 1940's, assumes that after the decay process begins, the particle is instantaneously at the outside edge of the nucleus, localized as a point, and moving outward with a definite classically defined velocity. Technically this model is a hybrid of quantum and classical physics as the tunnelling process is quantum mechanical and the interaction between the classical particle and the atom is treated through the time-dependent Schrödinger equation. The atom is always treated quantum mechanically, but the trajectory and propagation of the particle is treated classically so we sometimes refer to this as the classical treatment. The ionization probability predicted by

this theory agrees well with experiment (Levinger 1953; Fischbeck and Freedman 1975; Fischbeck and Freedman 1977).

Conceptually it is hard to imagine that a classical model should give the correct result. The α-decay process obeys an exponential decay law, meaning that for the case of a long half-life, its quantum mechanical wavefunction leaks very slowly out of the nucleus. This wavefunction has an abrupt wavefront followed by a long exponential tail and has been approximated well with a heuristic form (Breit 1959; van Dijk, Kataoka, and Nogami 1999). This heuristic form has been corroborated using an exact analytical model (van Dijk and Nogami 1999; van Dijk and Nogami 2002; van Dijk and Nogami 2004). The wavefront moves out with the classical velocity, but for long decay times the expectation value of the position of the particle initially moves very slowly, as most of the wavefunction remains in the nucleus. In the same vein, the nuclear charge number when treated classically changes abruptly from Z to $Z-2$, but in the wavefunction treatment would have the same slow change as the expectation value. The slow rates in the quantum mechanical treatment of the α-particle, suggests that the interaction would be adiabatic, with the atom only mildly perturbed by the passing wavefunction, leading to low excitation probabilities. However, as we said above the classical treatment agrees with the experiment so the process is not adiabatic.

Recently an attempt was made to accurately model this phenomenon with a proper time-dependent quantum mechanical (QM) treatment by Kataoka, et al. (Kataoka, Nogami, and van Dijk 2000; Kataoka 1998) (hereafter referred to as KNvD). In this work the classical α-particle propagation result was compared to two approximate QM models. The models are simplified, one dimensional versions of the problem. In their first QM model (model IIa), an electron is bound in the atom by a potential represented by the Pöschl-Teller potential (Pöschl and

Teller 1933; Flügge 1974) at the origin, in one dimension, with parameters such that there were 2 bound states for the electron. The α-particle, represented by the leaking wavefunction of the heuristic form, then interacts with the electrons through a delta-function and the probability of transition to the higher bound state or to the continuum of scattering states was calculated exactly, and with perturbation theory. In this model, the approximation was made that the α-particle's wavefunction was not affected by the transition. This approximation was made based on the α-particle being much more massive than the electron.

The second QM model of KNvD (model IIb) was similar in structure to their first QM model, but took account of the correlation between the α-particle and the electron and the excitation to scattering states is also accounted for, so this model is more complete. Because of the complexity of the second model it was only solved using first-order perturbation theory, which assumes that the interaction was weak. The two QM models in this work are consistent with each other in their prediction of the excitation probability, but differ from the classical model by giving a result between two and six orders of magnitude lower, depending on the interaction and binding strengths assumed. In this sense they agree with the adiabatic argument above, but not with the experimental result. This led to speculation that this excitation process could not be properly described with this wavefunction method (Nogami and van Dijk 2001). In the classical way of thinking, this is a single-particle event, with a single α-particle exciting a single electron, and it was thought that the ensemble of events described by the wavefunction did not properly describe the excitation.

A follow up work (van Dijk, Kiers, Nogami, Platt, and Spyksma 2003), used a more schematic model of the atom as simply a one dimensional, 2-level system centered around the origin where the interaction potential was represented by

a Gaussian form. The α-particle was treated both quantum mechanically as an incident wavepacket and classically as a spatially extended object. It is not treated as a decaying particle as in the KNvD work, but as a free particle incident on the atom from the left, along a straight line. There is no possibility of ionization in this model, as the interaction causes either a transition to the higher state or leaves the atom in the lower state. The wavepacket was assumed to be either in the form of a Gaussian or in the form of a wavefront with an exponentially decaying tail, mimicking the heuristic wavefunction for the α-particle. When treated quantum mechanically, the transition probabilities after a long time, for a given interaction strength, were found to be essentially independent of the size and shape of the wavepacket, although the intermediate time dependence is highly variable. The important result of this work was that when the incident particle was treated quantum mechanically, agreement with the classical point particle result was found. In the classical treatment of the extended particle, however, the predicted transition probabilities were highly dependent on the size of the particle and agreement with the classical point particle result occurred only for very narrow distributions. The narrow distributions are effectively point particles, so this agreement is not surprising. For wider distributions the interaction with the atom is adiabatic and very small transition probabilities are predicted.

The goal of the present work is to try to determine the reason for the discrepancy between the Migdal theory and the result from KNvD, especially considering that in the follow up work (van Dijk, Kiers, Nogami, Platt, and Spyksma 2003) there was no discrepancy. We apply the approximations made by KNvD to a schematic model of the particle-atom system, similar to that used in the follow up. We use one-dimensional models for simplicity, but the dimension can be considered as the radial coordinate when using partial waves. We also investigate

the form of the KNvD models, with some changes that make the models easier to solve. One change was to reduce the problem to only having one spatial variable, the coordinate of the α-particle, and another was to ignore excitation into scattering states, in other words the atom is an excitable two-level system. By applying the same approximations to the schematic model of the follow up work, as well as to the more realistic decay model of KNvD, we hoped to see what led to the wrong result. It was found that one of the approximations made in KNvD should indeed lead to incorrect results. It was also found that our version of KNvD's more exact second model does agree with the classical result.

This document is organized as follows: chapter 2 presents an extension we have made to a powerful numerical modelling method for solving the Schrödinger wave equation. This improved model is necessary for a fast and efficient treatment of the 2-level QM models used.

Chapter 3 further investigates the schematic model of the quantum excitation of an atom by the passage of a particle. The approximations used in KNvD are applied to a schematic model and comparisons are made with the classical result.

In chapter 4, an α-decay model is presented that has some simplifications on the KNvD model. We compare the new results with the previous results and with the classical theory.

Chapter 5 has some concluding remarks and suggestions for future work.

Chapter 2

Modelling Transitions

2.1 Introduction

An important part of modern quantum mechanics is the ability of computers to solve complex algorithms implemented to solve time-dependent wave equations that, lacking analytic solutions, must be solved numerically. In this chapter we present a further extension to a powerful algorithm recently updated by Moyer (Moyer 2003). This algorithm is capable of solving wave packet propagation problems in one dimension, for a one-channel system, under the influence of a potential. Moyer updated the Crank-Nicolson algorithm used by Goldberg (Goldberg, Schey, and Schwartz 1967) for wavepacket propagation by adding in the so-called Numerov approximation. With this approximation the accuracy of the calculations in the spatial increment is increased by three orders of the spatial step size.

Moyer also extended the algorithm to include transparent boundary conditions (TBCs). This special form of boundary conditions behaves essentially as a transparent or non-existent boundary whereby the propagating wave or energy will go right through without reflecting. This is important in problems that evolve slowly with time as a large amount of computational resources can be wasted on calculations in the spatial dimension, away from the interesting physics of the problem. An example of such a problem would be a wave packet slowly leaking away from a potential well at the origin. In this case the potential is localized

near the origin so it becomes unnecessary to calculate propagation of the wave far from the potential.

In this work, we extend the Moyer algorithm with the Numerov approximation and TBCs to allow it to solve N-channel transition problems. The model was also updated to allow for a non-homogeneous term in the Schrödinger equation that occurs when perturbation theory is applied to the coupled equations arising from quantum interactions. As a minor note, this formulation also includes the mass m as a parameter rather than removing it early in the derivation as was done in the previous derivation (Moyer 2003).

2.2 Formulation

The problem amounts to propagating the wavefunction $\Psi(x,t)$ forward in time from some initial condition, or more succinctly, finding $\Psi(x,t)$ at the next time step, based on the physics of the problem and its value at an earlier time. We need a numerical method to solve Schrödinger's equation of the form

$$\left(i\frac{\partial}{\partial t} - H\right)\Psi(x,t) = N\,(x,t)\,. \tag{2.1}$$

$N(x,t)$ is a non-homogeneous source or driving term and the Hamiltonian is

$$H = -\frac{1}{2m}\frac{\partial^2}{\partial x^2} + U(x,t). \tag{2.2}$$

The factor m is the mass, and the potential term $U(x,t)$ contains the atomic energies, the background α-particle potential, and the interaction potentials. Throughout this work we use atomic units so that $\hbar = 1$ and the electron mass and charge are also equal to 1. The units of length, mass and energy are the Bohr radius, the electron mass and 1 Hartree=27.21 eV, respectively. This leads to a speed of

light of $c = 137$ which is much larger than the speed we use for the particles in this work ($v \approx 1$). The units of time and speed are respectively 2.419×10^{-17} sec and 2.189×10^{8} cm/sec.

To adapt this model to N channels we use a matrix formulation. For each value of x and t, $\Psi(x,t)$ and $N(x,t)$ are N×1 vectors and H is an N×N matrix.

For the case of transition problems in this work, the Hamiltonian takes the specific form

$$\begin{aligned} H &= H_{kin} + H_0 + H_{int} && (2.3) \\ &= \sum_{i=1}^{\mathrm{N}} \left(\frac{p^2}{2m} + \epsilon_i \right) |i\rangle\langle i| + \sum_{i,j=1}^{N} V_{i,j}(x)|i\rangle\langle j|, && (2.4) \end{aligned}$$

where H_{kin} is the kinetic energy part of the Hamiltonian and H_0 simulates the N-level atom such that $H_0|i\rangle = \epsilon_i|i\rangle$ for $i = 1, \ldots, \mathrm{N}$ and $\langle i|j\rangle = \delta_{ij}$. H_{int} covers the interaction between the particle and the atom through the potential $V_{i,j}(x)$. Then $\Psi(x,t)$ takes the form $\Psi(x,t) = \sum_{i=1}^{\mathrm{N}} \psi_i(x,t)|i\rangle$. The $\psi_i(x,t)$'s are scalars for each x and t and the ket $|i\rangle$ is an N×1 vector of zeros except for a 1 in the i-th row, representing the i-th bound state.

Thus $U(x,t)$ in (2.2) is

$$U(x,t) = \sum_{i=1}^{\mathrm{N}} \epsilon_i|i\rangle\langle i| + \sum_{i,j=1}^{N} V_{i,j}(x)|i\rangle\langle j|. \qquad (2.5)$$

Inserting (2.2) into (2.1) and rearranging, we have

$$\begin{aligned} \left[i\frac{\partial}{\partial t} + \frac{1}{2m}\frac{\partial^2}{\partial x^2} - U(x,t) \right] \Psi(x,t) &= N(x,t) && (2.6) \\ \left[-\frac{1}{2m}\frac{\partial^2}{\partial x^2} + U(x,t) \right] \Psi(x,t) &= i\frac{\partial \Psi(x,t)}{\partial t} - N(x,t) && (2.7) \end{aligned}$$

We now make substitutions for the main functions in (2.7) by replacing $\Psi(x,t)$ and $N(x,t)$ by their averages over the time step Δt, and $\partial\Psi(x,t)/\partial t$ by the finite difference form:

$$\begin{aligned}
\Psi(x,t) &\rightarrow [\Psi(x,t)+\Psi(x,t+\Delta t)]/2 \\
N(x,t) &\rightarrow [N(x,t)+N(x,t+\Delta t)]/2 \\
\frac{\partial\Psi(x,t)}{\partial t} &\rightarrow [\Psi(x,t+\Delta t)-\Psi(x,t)]/\Delta t
\end{aligned}$$

This leads to

$$\left[-\frac{1}{2m}\frac{\partial^2}{\partial x^2}+U(x,t)-i\frac{2}{\Delta t}\right]y(x,t)=-i\frac{4}{\Delta t}\Psi(x,t)+M(x,t) \tag{2.8}$$

where

$$y(x,t)=\Psi(x,t)+\Psi(x,t+\Delta t) \tag{2.9}$$

and $M(x,t) = -[N(x,t)+N(x,t+\Delta t)]$. Equation (2.8) can be derived more rigourously as shown by Puzyin, et al. (Puzyin, Selin, and Vinitsky 2000).

Rearranging (2.8) further leads to

$$\frac{\partial^2}{\partial x^2}y(x,t)=\left[2mU(x,t)-i\frac{4m}{\Delta t}\right]y(x,t)+\left[i\frac{8m}{\Delta t}\Psi(x,t)+2mM(x,t)\right]. \tag{2.10}$$

We can proceed using the Numerov method since at a given time, the spatial dependence is of the form $y''(x)=g(x)y(x)+f(x)$. In this case

$$g(x,t) = 2mU(x,t)-i\frac{4m}{\Delta t} \tag{2.11}$$

$$f(x,t) = i\frac{8m}{\Delta t}\Psi(x,t)+2mM(x,t). \tag{2.12}$$

For the N-channel problem, $g(x,t)$ is an N×N matrix, while $f(x,t)$ is an N×1 vector, for each value of x and t.

We want the next order term over the regular centered-difference so we expand $y(x+h)$ and $y(x-h)$, where h is the spatial mesh size.

$$\begin{aligned} y(x+h) = y(x) &+ y'(x)h + \frac{1}{2}y''(x)h^2 + \frac{1}{3!}y'''(x)h^3 + \frac{1}{4!}y^{(4)}(x)h^4 \\ &+ \frac{1}{5!}y^{(5)}(x)h^5 + O(h^6) \end{aligned} \tag{2.13}$$

$$\begin{aligned} y(x+h) = y(x) &- y'(x)h + \frac{1}{2}y''(x)h^2 - \frac{1}{3!}y'''(x)h^3 + \frac{1}{4!}y^{(4)}(x)h^4 \\ &- \frac{1}{5!}y^{(5)}(x)h^5 + O(h^6) \end{aligned} \tag{2.14}$$

Adding the two gives

$$y(x+h) + y(x-h) = 2y(x) + y''(x)h^2 + \frac{2}{4!}y^{(4)}(x)h^4 + O(h^6), \tag{2.15}$$

where the first two terms on each side are the usual second order centered difference. We now compress the notation as follows: $y_j \equiv y(x_0 + jh)$ and similarly for $g(x)$ and $f(x)$. The factor j indexes the spatial steps from the left-most spatial grid point x_0. Then (2.15) becomes

$$y_{j+1} + y_{j-1} = 2y_j + y_j''h^2 + \frac{1}{12}y_j^{(4)}(x)h^4 + O(h^6). \tag{2.16}$$

Recognizing that $y_j^{(4)} = (g_j y_j + f_j)''$ and using the central difference method $\left[y_j''h^2 \approx y_{j+1} + y_{j-1} - 2y_j\right]$ again, we rewrite (2.16) as

$$\begin{aligned} y_j''h^2 = &\quad y_{j+1} + y_{j-1} - 2y_j \\ &- \frac{h^2}{12}\left[(g_{j+1}y_{j+1} + f_{j+1}) + g_{j-1}y_{j-1} + f_{j-1} - 2g_j y_j - 2f_j\right]. \end{aligned} \tag{2.17}$$

Substituting $y_j'' = g_j y_j + f_j$ into (2.17) and rearranging gives

$$\begin{aligned} \left(d_{j+1}y_{j+1} - \frac{h^2}{12}f_{j+1}\right) &+ \left(d_{j-1}y_{j-1} - \frac{h^2}{12}f_{j-1}\right) \\ &- 2\left(d_j y_j - \frac{h^2}{12}f_j\right) = (g_j y_j + f_j)\,h^2, \end{aligned} \tag{2.18}$$

where $d_j = I - \frac{h^2}{12} g_j$, and I is the identity matrix of the appropriate size.

Defining $w_j \equiv d_j y_j - \frac{h^2}{12} f_j$, (2.18) can be rewritten

$$w_{j+1} + w_{j-1} = \left[2I + h^2 g_j d_j^{-1}\right] w_j + h^2 d_j^{-1} f_j. \tag{2.19}$$

We emphasize that the order of multiplication here (and throughout) is important as both g_j and d_j are N×N matrices.

Now suppose we can represent w_{j+1}, the next value of w to the right in space as a linear function of the value to its left:

$$w_{j+1} = e_j w_j + q_j. \tag{2.20}$$

Substituting (2.20) into (2.19) leads to

$$\begin{aligned} w_{j+1} = & \left[2I + h^2 g_{j+1} d_{j+1}^{-1} - e_{j+1}\right]^{-1} w_j \\ & + \left[2I + h^2 g_{j+1} d_{j+1}^{-1} - e_{j+1}\right]^{-1} \left(q_{j+1} - h^2 d_{j+1}^{-1} f_{j+1}\right). \end{aligned} \tag{2.21}$$

Comparing this with (2.20) we see that

$$e_j = \left[2I + h^2 g_{j+1} d_{j+1}^{-1} - e_{j+1}\right]^{-1} \tag{2.22}$$

$$e_j + e_{j-1}^{-1} = 2I + h^2 g_j d_j^{-1}, \tag{2.23}$$

where (2.23) was found from (2.22) by rearranging terms and shifting the index by 1.

Similarly

$$\begin{aligned} q_j &= e_j \left(q_{j+1} - h^2 d_{j+1}^{-1} f_{j+1}\right) \\ q_j &= e_{j-1}^{-1} q_{j-1} + h^2 d_j^{-1} f_j. \end{aligned} \tag{2.24}$$

We can rearrange (2.20)

$$w_{j-1}^n = \left(e_{j-1}^n\right)^{-1}\left(w_j^n - q_{j-1}^n\right), \tag{2.25}$$

where the superscript n has been added to keep track of the time steps such that $t_n = t_0 + n\Delta t$. These superscripts are always assumed, but are only stated explicitly when necessary for clarity.

For rigid walls $w_0^n = 0$ for all n, but w_j^n and q_{j-1}^n in (2.25) are not necessarily equal. Therefore $(e_0^n)^{-1}$ must force it to be zero, resulting in e_0^n taking the form of a diagonal matrix with all diagonal elements being infinity and

$$e_1 = 2I + h^2 g_1 d_1^{-1}. \tag{2.26}$$

For a spatial dimension divided into J steps, e_j can be found by forward recursion from $j = 1$ to $j = J$. If the potential is time-independent, g_j and d_j do not vary with time and the e_j's only need to be calculated once.

The values of q_j^n are also found in a forward recursion. From (2.24) we see that

$$q_1^n = e_0^{-1} q_0^n + h^2 d_1^{-1} f_1^n. \tag{2.27}$$

From the above arguments though, $e_0^{-1} = 0 \times I$ so if q_0^n is finite $q_1^n = h^2 d_1^{-1} f_1^n$. Note that f_j^n changes at each time step, so q_j^n must be calculated at each time step regardless of the time-dependence of the potential.

We are now prepared to calculate the values of w_j^n. From (2.20), $w_{j+1}^n = e_j w_j^n + q_j^n$, but because of the form of e_0 assumed above we cannot start from the $j = 0$ boundary since we would have $\infty \times 0$. Using (2.25), starting from $j = J$ and noting that $w_J^n = 0$ on the right boundary as well, we can calculate w_j^n in a backwards recursion down to $j = 1$, with $w_0^n = 0$ on the left boundary as above.

After w_j is calculated, we can unfold all of the transformations we have applied to recover the wavefunction at the next time step. Start by rewriting (2.9)

$$y_j^n \equiv \Psi_j^{n+1} + \Psi_j^n \tag{2.28}$$

$$\Psi_j^{n+1} = y_j^n - \Psi_j^n \tag{2.29}$$

and rearranging $w_j \equiv d_j y_j - \frac{h^2}{12} f_j$ to read $y_j^n = \left(d_j^n\right)^{-1}\left(w_j^n + \frac{h^2}{12} f_j n\right)$.

Now, from (2.12) $f_j^n \equiv i\frac{8m}{\Delta t}\Psi_j^n + 2mM_j^n$ so finally

$$\Psi_j^{n+1} = \left(d_j^n\right)^{-1}\left(w_j^n + i\frac{2h^2m}{3\Delta t}\Psi_j^n + \frac{h^2m}{6}M_j^n\right) - \Psi_j^n, \tag{2.30}$$

and we have an equation for $\Psi(x,t)$ at the next time step. This cycle is repeated allowing $\Psi(x,t)$ to be easily found over many time steps.

2.3 Transparent Boundary Conditions

The derivation and addition of the transparent boundary conditions (TBCs) is quite involved so we included it by reference to Moyer's paper (Moyer 2003). The basic idea with TBCs is to limit the computational domain so that simulations run faster. The accuracy can then also be improved since there is additional free memory. In the present formulation without the TBCs we can think of our boundary conditions as rigid walls where the solution is forced to go to zero at these points. This causes reflections (in the same way as a string fixed to a wall), and is not ideal for long propagation times since the energy being propagated may reflect off the rigid wall and interfere with the problem. Because of these reflections it is necessary to keep the propagating wave and potential regions far away from the walls and consequently there is a large computational domain going to waste. With a TBC the wall can be moved much closer to the region of interest

in the problem as the propagating wave does not reflect off this type of wall, but effectively goes right through it.

In this formulation the TBCs enter through the boundary conditions w_0^n and w_J^n shown earlier. Moyer's formulation stays identical since TBCs are only applied away from any interaction or potential regions. All matrices in the present formulation then become diagonal matrices since there is no coupling between channels at the TBC, and so TBCs are essentially just applied to each channel individually.

All formulas for the TBCs can be applied as stated in Moyer's paper, but note that since we have included the mass m explicitly in this formulation, Moyer's variable c for the TBCs becomes $c = I - i\frac{\lambda m}{3}d^{-1}$.

2.4 Verification of Numerical Method

The homogeneous model ($N(x,t) = 0$) will be verified for a 2-channel problem by recalculating recently published results (van Dijk, Kiers, Nogami, Platt, and Spyksma 2003), which used the Crank-Nicolson method and a fast Fourier transform method (Tal-Ezer and Kosloff 1984; Leforestier 1991). For more on 2-channel problems see the well-written text by Griffiths (Griffiths 1995). This problem is similar to the one we investigate in the next chapter. We consider a wavepacket impinging on a quantum 2-level system from the left and interacting through a potential $V(x)$. The system is initially in the ground state with energy $\epsilon_1 = 0$ and has a possibility of being excited to energy $\epsilon_2 = 1$ by the passage of the wavepacket.

We begin with the form of the wavefunction

$$\Psi(x,t) = \psi_1(x,t)|1\rangle + \psi_2(x,t)|2\rangle. \tag{2.31}$$

Continuing with the model of van Dijk, et al. we substitute (2.31) into (2.3) and (2.1) with $N(x,t) = 0$. This leads to the following coupled equations for $\psi_i(x,t)$ and $\psi_j(x,t)$ $(i,j = 1 \text{ or } 2)$

$$\left(i\frac{\partial}{\partial t} + \frac{1}{2m}\frac{\partial^2}{\partial x^2} - \epsilon_i\right)\psi_i(x,t) = V(x)\psi_j(x,t), \quad i \neq j. \tag{2.32}$$

The interaction between the wavepacket and the system is governed by the potential $V(x) = V_{1,2}(x) = V_{2,1}(x) = \lambda(\beta/\sqrt{\pi})e^{-\beta^2 x^2}$ and $V_{i,i}(x) = 0$.

We assume the initial condition at $t = t_0$,

$$\psi_1(x,t_0) = f(x - x_0)e^{ik(x-x_0)}, \quad \psi_2(x,t_0) = 0. \tag{2.33}$$

The function $f(x - x_0)e^{ik(x-x_0)}$ specifies the initial shape of the incident wave packet. It is localized around $x = x_0 \ll 0$ and moves with initial speed $v = k/m > 0$ toward the origin. For $f(x - x_0)$ we assume the Gaussian form

$$f(x - x_0) = (2\pi\sigma_0^2)^{-1/4} \exp\left[-\left(\frac{x - x_0}{2\sigma_0}\right)^2\right], \tag{2.34}$$

where $\sigma_0 > 0$ is the initial width, and x_0 is the initial center of the wavepacket. We assume the same values for the various parameters as those used in the work of van Dijk et al. (van Dijk, Kiers, Nogami, Platt, and Spyksma 2003). Specifically we choose $v = 1$, $m = 100$, and $\beta = 1$ and vary the parameters σ_0 and x_0 according to the problem. We choose $x_0 \ll -\sigma_0$ and $x_0 \ll -1/\beta$ so that the incident wave packet at $t = t_0$ is well outside the interaction region. The initial time is $t_0 = x_0/v$, chosen such that a non-interacting wavepacket would be centered at the origin at $t = 0$.

Throughout this chapter and the next we assume $\epsilon_1 = 0$ and $\epsilon_2 = 1$. The mass is set to $m = 100$ to simulate the α particle being much more massive than the

electrons. With the velocity typically around 1, the kinetic energy for the incident particle is then $mv^2/2 \approx 50$ and is much larger than the excitation energy between the 2 states of the atom.

The probability for the transition 1→2 is given by

$$P_{21}(t) = \int_{-\infty}^{\infty} |\psi_2(x,t)|^2 dx, \tag{2.35}$$

which starts with $P_{21}(t_0) = 0$ and approaches a constant as $t \to \infty$.

Figure 2.1 shows the result of our calculations, which agrees with Figure 2 of van Dijk et al. (van Dijk, Kiers, Nogami, Platt, and Spyksma 2003). Our σ_0 corresponds to Δ in that work. We see the identical behaviour, with the transition probability for large t virtually independent of the wavepacket size or starting position. Our results converge to the same result as in the paper. The time dependence around $t = 0$ also shows the same form. The numerical method described in this chapter appears to be capable of solving these types of problems. The non-homogeneous model ($N(x,t) \neq 0$) will be tested in chapter 3.

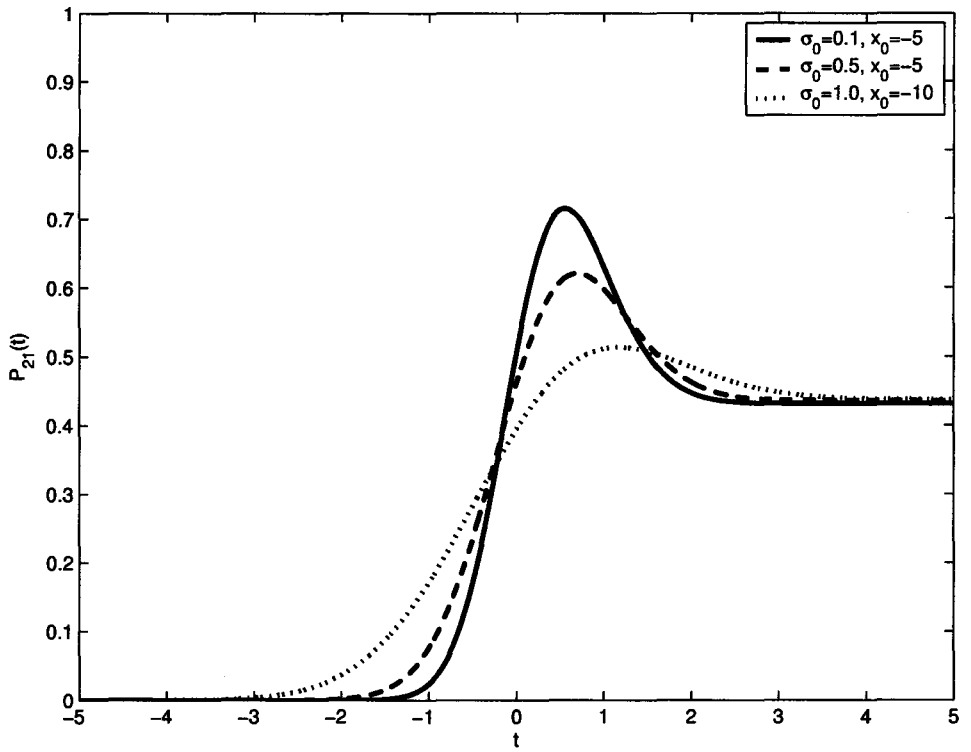

Figure 2.1: Verification of numerical method by a new calculation of published results for a wavepacket interacting with a 2-level system. $\lambda = 2$, $v = \beta = 1$

Chapter 3

Excitation by the Passage of a Particle

3.1 Introduction

We consider a schematic model of the excitation process where a 2-level atom is located at the origin and a particle impinges on it from the left, with the possibility of exciting it from the lower state to the higher. The particle can be a point particle, or extended in space, or a quantum mechanical wavepacket. For the spatially extended particle, we also consider the case where the particle's distribution changes with time. The point particle and the extended particle follow classical trajectories through space with well-defined velocities. We look at different forms of the classically behaving particles to see if we can recreate the independence on particle shape seen in the recent work by van Dijk, et al. (van Dijk, Kiers, Nogami, Platt, and Spyksma 2003).

The schematic model itself is the same as the follow up work on the KNvD (Kataoka, Nogami, and van Dijk 2000) result by van Dijk, et al. (van Dijk, Kiers, Nogami, Platt, and Spyksma 2003), although we also include spreading of the size of the wavepacket for the classical extended particles. We apply the approximations used by KNvD to this schematic model with the hope of finding where the discrepancy lies. The first part of this chapter, Approximation A, corresponds to model IIa of KNvD and the second part, Approximation B, corresponds to their model IIb.

We start from the Schrödinger equation as before. We consider a situation such that the atom is initially in the ground state $|1\rangle$. A wave packet is incident from the left and it interacts with the atom which is fixed at the origin. The atom may be excited to level $|2\rangle$. We solve the time-dependent Schrödinger equation

$$\left(i\frac{\partial}{\partial t} - H\right)\Psi(x,t) = 0, \tag{3.1}$$

where the Hamiltonian is given by

$$\begin{aligned} H &= H_{kin} + H_0 + H_{int} && (3.2)\\ &= \sum_{i=1}^{2}\left(\frac{p^2}{2m} + \epsilon_i\right)|i\rangle\langle i| + \sum_{i,j=1;i\neq j}^{2} V_{i,j}(x)|i\rangle\langle j|. && (3.3) \end{aligned}$$

H_{kin} is the kinetic energy part of the Hamiltonian and H_0 simulates the 2-level atom such that $H_0|i\rangle = \epsilon_i|i\rangle$ for $i = 1, 2$ and $\langle i|j\rangle = \delta_{ij}$. H_{int} covers the interaction potential between the particle and the atom. This potential, centered around the origin, is given by

$$V(x) = V_{1,2}(x) = V_{2,1}(x) = \lambda(\beta/\sqrt{\pi})e^{-\beta^2 x^2}, \tag{3.4}$$

where $1/\beta$ determines the potential width, λ the potential strength and the diagonal terms of the potential $V_{i,i}(x) = 0$.

We proceed by testing two different models using different forms of $\Psi(x,t)$. We label these two approximations, A and B, and they are similar to the KNvD models IIa and IIb, respectively. Model A assumes that the α-particle wavefunction is unaffected by the interaction with the atom and uses a simplified form of $\Psi(x,t)$. Model B, accounts for changes to the α-particle wavefunction, by using the proper x and t dependent form for the states of $\Psi(x,t)$. Since this model is similar, but simpler we hope to shed some light on which approximations could have caused problems in models IIa and IIb.

3.2 Approximation A

In approximation A, we assume a wavefunction of the form

$$\Psi_A(x,t) = \phi(x,t)[c_1(t)|1\rangle + c_2(t)|2\rangle], \tag{3.5}$$

where $\phi(x,t)$ is determined by

$$\left(i\frac{\partial}{\partial t} + \frac{1}{2m}\frac{\partial^2}{\partial x^2}\right)\phi(x,t) = 0. \tag{3.6}$$

The assumption here is that the spatial distribution of the wavefunction is not at all affected by an interaction with the atom.

Substituting (3.5) into (3.1) with H as given in (3.2) leads to

$$\begin{aligned}\phi(x,t)i\frac{\partial}{\partial t}\left[c_1(t)|1\rangle + c_2(t)|2\rangle\right] &= \phi(x,t)\left[\epsilon_1 c_1(t)|1\rangle + \epsilon_2 c_2(t)|2\rangle\right] \\ &+ \phi(x,t)V(x)\left[c_1(t)|2\rangle + c_2(t)|1\rangle\right].\end{aligned} \tag{3.7}$$

We can multiply (3.7) by $\phi^*(x,t)$ and integrate over all x to obtain the following coupled equations for $c_i(t)$ with $i = 1, 2$ and $i \neq j$

$$\left(i\frac{\partial}{\partial t} - \epsilon_i\right)c_i(t) = W_A(t)c_j(t) \tag{3.8}$$

where

$$W_A(t) = \int_{-\infty}^{\infty}\rho(x,t)V(x)dx, \tag{3.9}$$

and $\rho(x,t) = \phi^*(x,t)\phi(x,t)$. Note that any phase information for the α-particle is now lost since this is the only place the α-particle wavefunction enters the equations and $\rho(x,t)$ is the magnitude squared of the wavefunction.

We continue by rewriting $c_{1,2}(t)$ as $c_{1,2}(t) = \gamma_{1,2}(t)e^{-i\epsilon_{1,2}t}$, so that (3.8) simplifies to

$$\frac{\partial}{\partial t}\gamma_1(t) = -iW_A(t)\gamma_2(t)e^{i(\epsilon_1-\epsilon_2)(t-t_0)} \tag{3.10}$$

$$\frac{\partial}{\partial t}\gamma_2(t) = -iW_A(t)\gamma_1(t)e^{i(\epsilon_2-\epsilon_1)(t-t_0)}, \tag{3.11}$$

where t_0 is the initial time. Note that all spatial information in the problem is contained within the integral in $W_A(t)$.

The probability of transition to state 2 for the coupled equation (CE) solution within approximation A, as a function of time is then

$$P_{21}^{A,CE}(t) = |c_2(t)|^2 = |\gamma_2(t)|^2. \tag{3.12}$$

To proceed we must define $\phi(x,t)$. We use the form given in Liboff (Liboff 1991) for a Gaussian wavepacket evolving, or spreading, in time.

$$\begin{aligned}\phi(x,t) &= \left(2\pi\sigma_0^2\right)^{-1/4}(1+it/\tau)^{-1/2}\exp\left[i\frac{\tau}{t}\left(\frac{x-x_0}{2\sigma_0}\right)^2\right] \\ &\times \exp\left[-\frac{(i\tau/(4\sigma_0^2 t))(x-x_0-kt/m)^2}{1+it/\tau}\right]\end{aligned} \tag{3.13}$$

In (3.13), $\tau = 2m\sigma_0^2$, x_0 is the initial center of the wavepacket and k is the momentum wavenumber such that $kt/m = vt$. Since $\hbar = 1$, k is identical to the momentum. The wavepacket width is set by σ_0 and the mass $m = 100$ to simulate the heavy α particle.

We can now calculate $\rho(x,t)$ so that we can find $W_A(t)$

$$\rho(x,t) = |\phi(x,t)|^2 = \frac{1}{\sigma_t\sqrt{2\pi}}\exp\left[-\frac{(x-x_t)^2}{2\sigma_t^2}\right], \tag{3.14}$$

where $x_t = x_0 + kt/m = x_0 + vt$. The new time dependent width $\sigma_t = \sigma_0\left(1+t^2/\tau^2\right)^{1/2} = \sigma_0\left(1+t^2/(4m^2\sigma_0^4)\right)^{1/2}$ so $\sigma_t^2 = \sigma_0^2 + t^2/(4m^2\sigma_0^4)$.

Inserting (3.14) and (3.4) into (3.9) gives

$$W_A(t) = \frac{\lambda}{\sigma_t'\sqrt{2\pi}} \exp\left[-\frac{1}{2}\left(\frac{x_t}{\sigma_t'}\right)^2\right] \tag{3.15}$$

where $\sigma_t' = \sqrt{\sigma_t^2 + 1/(2\beta^2)}$

The coupled equations (3.10) and (3.11) are solved using the internal Matlab function *ode45* and results are shown in the next section. The function *ode45* is an step-size adjusting Runge-Kutta integration method designed to solve coupled differential equations of type (3.10) and (3.11).

3.2.1 Approximation A: Perturbation theory

For small potential strength λ, (3.8) should be approximately solvable using perturbation theory. Begin by assuming

$$c_1(t) = e^{-i\epsilon_1(t-t_0)}, \tag{3.16}$$

and insert this into (3.8)

$$\left(i\frac{d}{dt} - \epsilon_2\right) c_2(t) = W_A(t)e^{-i\epsilon_1(t-t_0)}. \tag{3.17}$$

Then $c_2(t)$ is determined by rearranging (3.17) and integrating over the desired time interval:

$$c_2(t) = -ie^{-i\epsilon_2(t-t_0)} \int_{t_0}^{t} W_A(t')e^{i(\epsilon_2-\epsilon_1)(t'-t_0)}dt'. \tag{3.18}$$

Equation (3.18) was calculated numerically using Simpson's rule. Note that $c_2(t_0) = 0$.

The probability of transition is found in the same way as before:

$$P_{21}^{A,PT}(t) = |c_2(t)|^2. \tag{3.19}$$

3.2.2 Results of Approximation A

We now look at results for the coupled equations (3.10), (3.11) and for the perturbation theory (3.18). The following parameters are constant between the different figures: $\beta = 1$, $m = 100$, $\epsilon_1 = 0$, $\epsilon_2 = 1$. For Figures 3.1, 3.2, 3.3, and 3.4 we look at a range of initial widths σ_0, with $v = 1$, for 2 strengths of the potential, λ. The results are plotted for a range of the starting wavepacket center, x_0. By decreasing x_0, the incident particle starts farther away from the atom (at the origin), and so evolves for a longer time before reaching it.

A comparison is made with the non-spreading (subscript ns) particle result obtained for the simpler version of $\rho_{ns}(x,t)$ inserted into the coupled equations through (3.9):

$$\rho_{ns}(x,t) = \rho_{ns}(x) = \frac{1}{\sigma_0\sqrt{2\pi}} \exp\left[-\frac{(x-x_0)^2}{2\sigma_0^2}\right]. \tag{3.20}$$

The non-spreading particle result after $t = \infty$ is independent of x_0 since the width of the particle does not change with time.

The classical point particle model is dealt with more thoroughly in the next chapter, but amounts to substituting $V(vt)$ for $W_A(t)$, (or $\rho(x,t) = \delta(vt)$ where vt is the position of the point particle at time t), in (3.9). Since the interacting particle is assumed to have no size, this corresponds to $\sigma_0 = 0$. The expected result for the transition probability at $t = \infty$ is $P_{21}^{point} = 0.006044$ for $\lambda = 0.1$ and $\beta = 1$. For $\lambda = 2$ and $\beta = 1$, $P_{21}^{point} = 0.44526$. Figures 3.1 and 3.2 correspond to $\lambda = 0.1$ and we see a trend towards the classical result as σ_0 decreases to 0.1. For σ_0 smaller than 0.1, the wavepacket broadens too quickly and the transition probability does not approach the classical result. A similar pattern is seen for Figures 3.3 and 3.4 with $\lambda = 2$.

The perturbation theory (PT) result is given in Figures 3.1 and 3.2 where $\lambda = 0.1$, but not in Figures 3.3 and 3.4 as $\lambda = 2$ is too large and the perturbation theory approximation breaks down. For Figures 3.1 and 3.2 there is very good agreement between the results of the coupled equations and PT with better results for smaller σ_0.

The results are close to the non-spreading particle result, as shown in Figure 3.2, for larger initial widths σ_0, since a larger packet spreads less rapidly. For narrower packets, as in Figure 3.1, the packet spreads more rapidly and so is much wider than its non-spreading counterpart when it reaches the potential near the origin, leading to a lower transition probability. As the wavepacket width is increased the interaction becomes adiabatic and the transition probability tends towards zero. For clarity in Figures 3.1 and 3.3, only one line is plotted for the non-spreading result as the values for all three cases of σ_0 ($\sigma_0 = 0.001, 0.01, 0.1$) are the same in the first two significant digits. The reason for this is that as σ_0 decreases for the non-spreading case, the wavepacket approaches a δ-function potential ($\sigma_0 = 0$) and the transition probability values are asymptotic to the point particle limit.

In all cases the physics breaks down when the starting point x_0 is too small as a portion of the wavepacket is already in the interaction region. In most cases this is seen as a rapid decrease in $P_{21}(\infty)$.

Figure 3.5 shows a comparison of the percentage difference between the result of the coupled equation solution and the PT solution for two different initial wavepackets and starting positions, and a range of velocities. As shown by the arrows the 10% and 20% points are similar in each case and we see that reliable results depend greatly on the velocity. From this result we see that for $v = 1$ as used above, the difference would be very great at $\lambda = 2$.

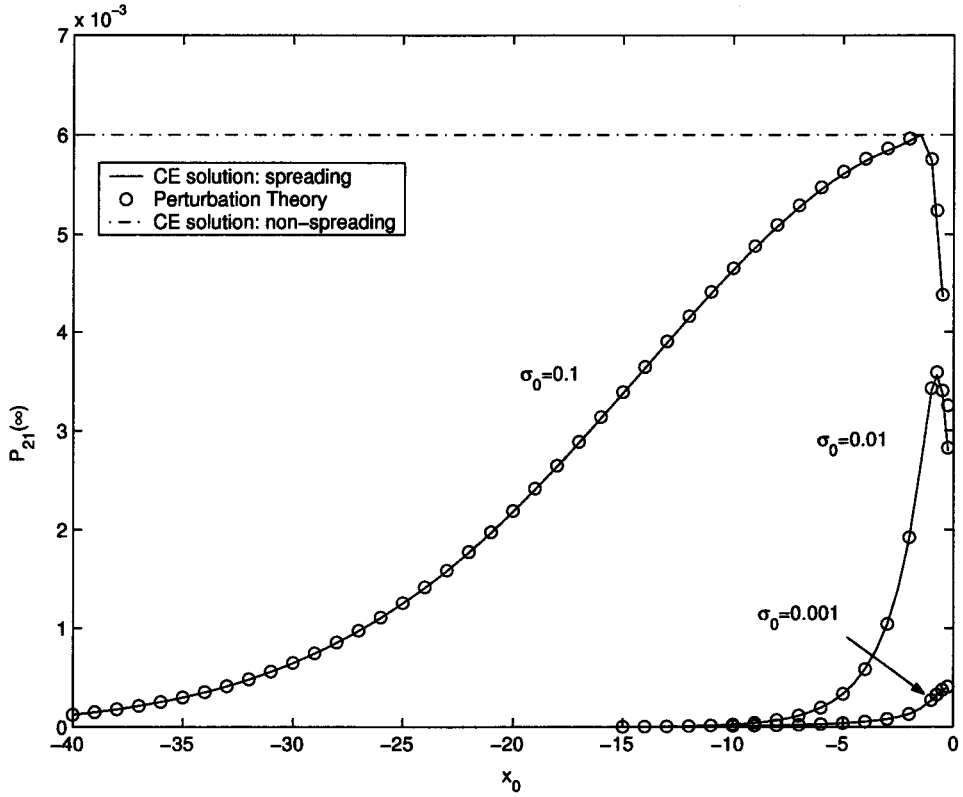

Figure 3.1: Comparison of $t = \infty$ transition probabilities, $P_{21}(\infty)$, for CE solution and perturbation theory of the spreading particle, with the CE solution for the non-spreading particle for a range of starting positions x_0. $\lambda = 0.1$. For non-spreading line $\sigma_0 = 0.001, 0.01, 0.1$.

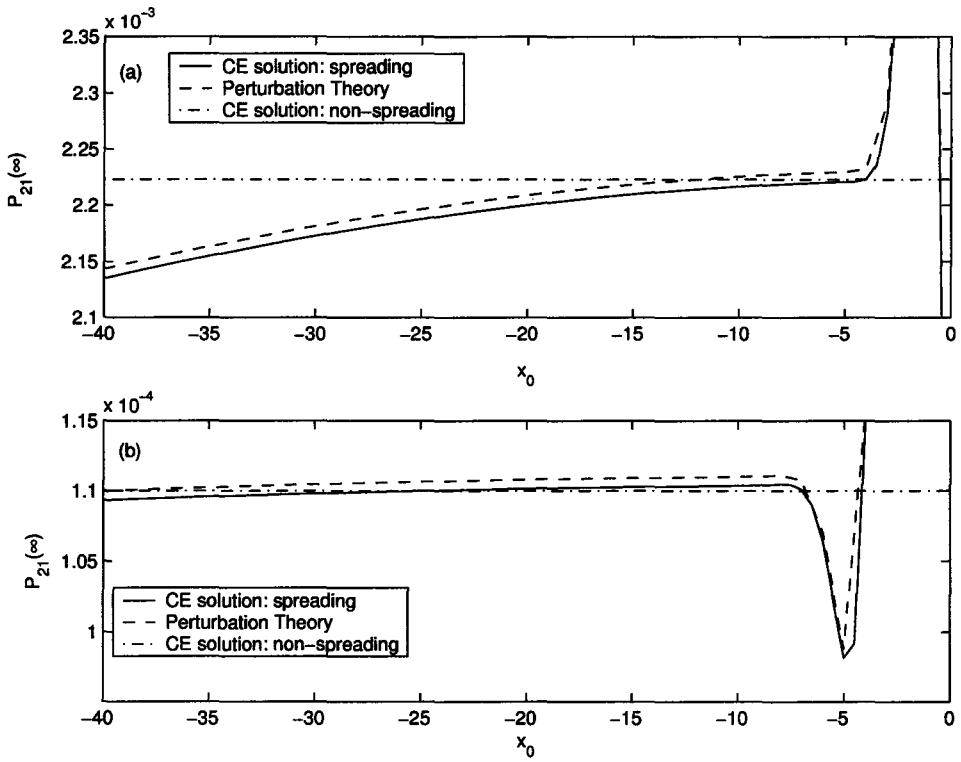

Figure 3.2: Comparison of $t = \infty$ transition probabilities, $P_{21}(\infty)$, for CE solution and perturbation theory of the spreading particle, with the CE solution for the non-spreading particle for a range of starting positions x_0. $\lambda = 0.1$, (a) $\sigma_0 = 1$, (b) $\sigma_0 = 2$.

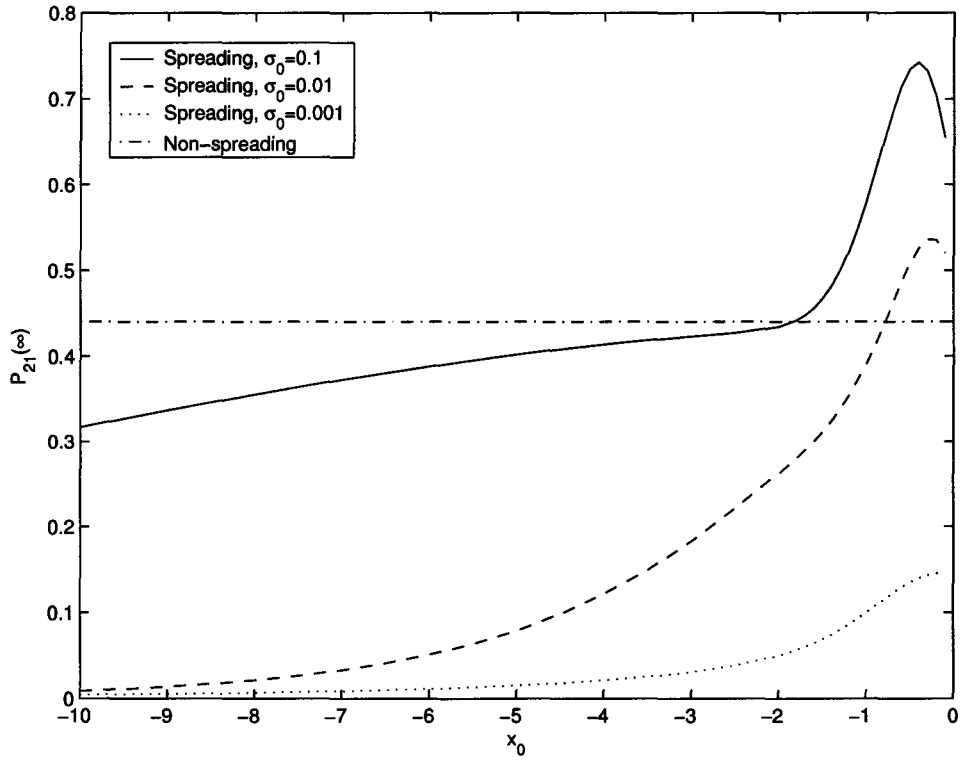

Figure 3.3: Comparison of $t = \infty$ transition probabilities, $P_{21}(\infty)$, for CE solution of the spreading particle, with the CE solution for the non-spreading particle for a range of starting positions x_0. $\lambda = 2$. For non-spreading line $\sigma_0 = 0.001$, 0.01, 0.1.

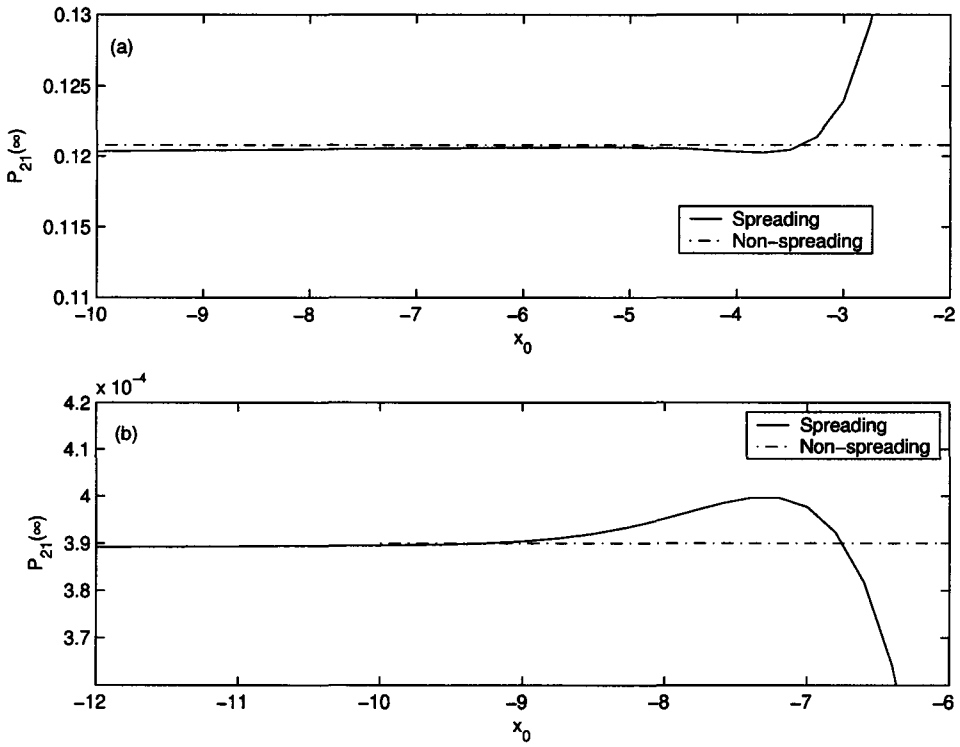

Figure 3.4: Comparison of $t = \infty$ transition probabilities, $P_{21}(\infty)$, for CE solution of the spreading particle, with the CE solution for the non-spreading particle for a range of starting positions x_0. $\lambda = 2$, (a) $\sigma_0 = 1$, (b) $\sigma_0 = 2$.

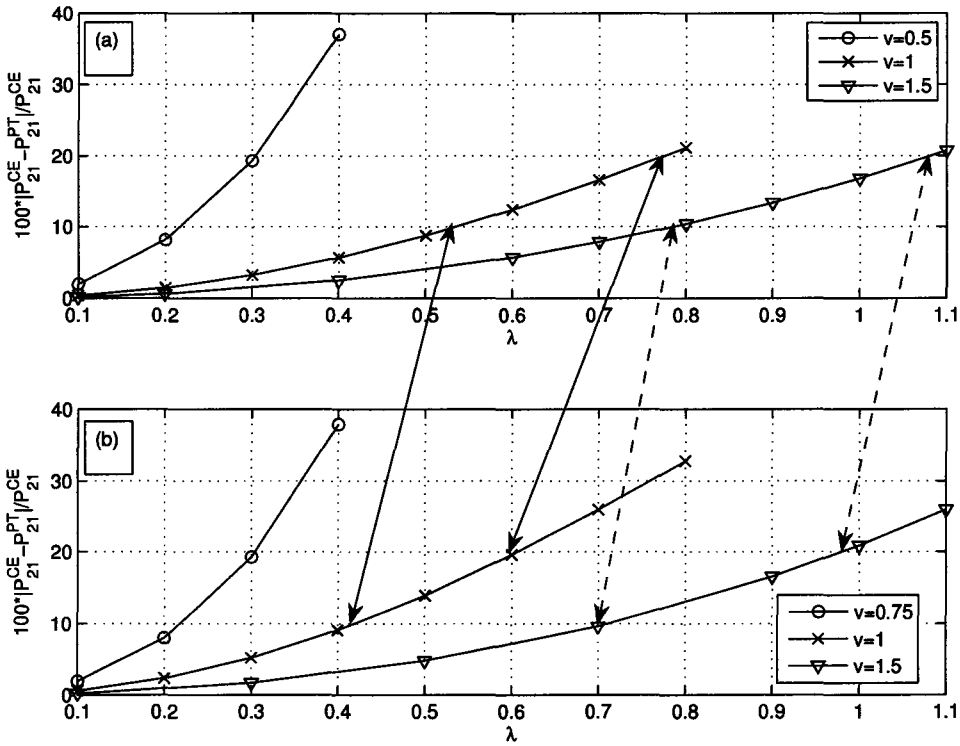

Figure 3.5: Percentage difference in transition probability between CE solution and 1st order PT, using the spreading particle and varying the potential strength λ. (a) $\sigma_0 = 0.1$, $x_0 = -10$, $m = 100$, (b) $\sigma_0 = 2$, $x_0 = -30$, $m = 100$.

3.3 Approximation B

This approximation resembles model IIb of KNvD in that the general form of the wavefunction is used. The particle is treated as a quantum wavepacket rather than as a spatially extended wave. The resulting equations are not solved exactly, they are solved using perturbation theory. Since PT worked well for the potential strength $\lambda \leq 0.1$ in the previous section, we can be confident in applying perturbation theory here. The general form of the wavefunction is

$$\Psi(x,t) = \psi_1(x,t)|1\rangle + \psi_2(x,t)|2\rangle. \tag{3.21}$$

Putting (3.21) and the Hamiltonian (3.2) into the time-dependent Schrödinger equation (3.1) leads to the coupled equations (seen earlier in chapter 2, (2.32)):

$$\left(i\frac{\partial}{\partial t} + \frac{1}{2m}\frac{\partial^2}{\partial x^2} - \epsilon_i\right)\psi_i(x,t) = V(x)\psi_j(x,t), \quad i \neq j. \tag{3.22}$$

Begin by assuming the initial conditions

$$\psi_1(x,t) = \phi(x,t)e^{-i\epsilon_1(t-t_0)}, \quad \psi_2(x,t) = 0. \tag{3.23}$$

where $\phi(x,t)$ is the same as in Approximation A, (3.13). By first-order PT then, after substituting (3.23) into (3.22), $\psi_2(x,t)$ is found by solving

$$\left(i\frac{\partial}{\partial t} + \frac{1}{2m}\frac{\partial^2}{\partial x^2} - \epsilon_2\right)\psi_2(x,t) = V(x)\phi(x,t)e^{-i\epsilon_1(t-t_0)}. \tag{3.24}$$

This equation is similar in form to the one solved in chapter 2, but now is only 1 channel (N=1). It can thus be solved using the non-homogeneous formulation presented in chapter 2.

The initial condition is $\psi_2(x,t_0) = 0$. The transition probability for $1 \rightarrow 2$ in this approximation is given by

$$P_{21}^B(t) = \int_{-\infty}^{\infty} |\psi_2(x,t)|^2 dx. \tag{3.25}$$

Figure 3.6 shows a new calculation, using this method, of the result reported by van Dijk, et al. (van Dijk, Kiers, Nogami, Platt, and Spyksma 2003) in Figure 1 of that paper. In that work the results were obtained using a more complicated 2-channel model which solved the coupled equations exactly, but we see here that the behaviour around $t = 0$ and results for $P_{21}(\infty)$ can be obtained using a simpler 1-channel model, if the potential strength λ is kept small. Recall that our σ_0 is Δ in the quoted paper.

The expected result is $P_{21}(\infty) = 0.00607$, so the difference is less than 10%, which is acceptable for a perturbative method. Agreement should be even better with $\lambda < 0.1$. We see also that $P_{21}(t = \infty)$ is essentially independent of the wavepacket width σ_0. Recall that the classical result for this value of $\lambda = 0.1$ is $P_{21}^{point} = 0.006044$.

Approximation B clearly captures enough of the physics to give accurate predictions. It agrees with the classical result and with exact quantum mechanical calculations. The issue appears to be with the form of the wavefunction used in Approximation A (and hence KNvD model IIa). This calculation was done partly as a test of the non-homogeneous formulation and partly to mimic model IIb of KNvD where PT was used in solving the coupled equations. Showing that the non-homogeneous formulation works in this case strengthens our confidence in applying it to the more rigorous model in the next chapter.

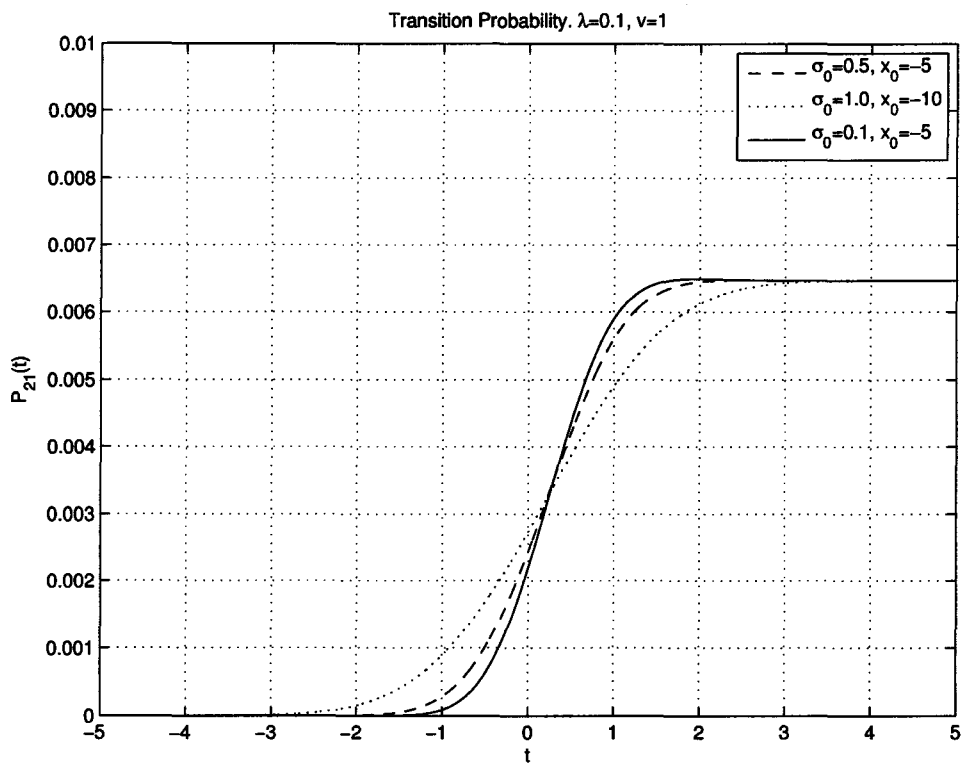

Figure 3.6: Calculation by a new method of van Dijk, et al. [van Dijk 03] Figure 1, using perturbation theory and a 1-channel non-Homogeneous version of the Schrodinger equation.

Chapter 4

Excitation Caused by α-Decay of the Nucleus

4.1 Introduction

In this chapter we consider the incident particle not as a Gaussian wave packet as in the previous chapter, but as a wavepacket slowly leaking out of the nucleus. The problem is posed for the spatial region $x > 0$ corresponding to the radial direction away from the nucleus. The potential $V(x)$ in this case simulates the α-particle interaction with the atom and so its range is on the atomic scale.

We again consider two different versions of the model, similar to the last chapter, as well as the classical model for comparison. One version again corresponds to KNvD model IIa which we dub here the Factorization Approximation. The second model uses the general form of the wavefunction with the solution to the coupled equations obtained using perturbation theory, corresponding to KNvD model IIb.

This model is much closer to the KNvD model than that of the last chapter, but has been simplified. This model contains only one spatial variable corresponding to the α-particle and does not contain the electron coordinate explicitly. The model considers only excitation to a higher state, while coupling to scattering states is not accounted for. It is hoped that the simplification will allow a more

accurate and transparent solution, possibly leading to an explanation of where the approximations in KNvD went wrong. The details of the α-particle's behaviour within the nucleus are ignored here as that is on a much smaller scale than the rest of the problem and would introduce difficulty into the numerical solution if the two different length scales are introduced into the same problem. A heuristic version of the α-particle wavefunction is assumed which simulates the slow decay of the particle from the nucleus, in this case located at the origin. Since there is no interaction between the α-particle and the atom while it is still in the nucleus the potential is chosen so that it is zero at the origin.

4.2 Model

To treat this problem properly we solve the time-dependent Schrödinger equation for the wavefunction $\Psi(x,t)$ for the atom-α particle system.

$$\left(i\hbar\frac{\partial}{\partial t} - H\right)\Psi(x,t) = 0. \tag{4.1}$$

The Hamiltonian for this problem takes the form

$$H = H_\alpha + H_{\text{atom}} + H_{\text{int}}, \tag{4.2}$$

where

$$H_\alpha = \frac{p^2}{2m} + U_\alpha, \quad H_{\text{atom}} = \sum_i \epsilon_i |i\rangle\langle i|, \quad H_{\text{int}} = \sum_{i,j=1;i\neq j}^{2} V_{i,j}(x)|i\rangle\langle j|. \tag{4.3}$$

H_α describes the behaviour of the α particle, H_{atom} simulates the two-state atom and H_{int} covers the interaction between the α-particle and the atom through the interaction potential $V(x)$. In this work we only consider the off diagonal components of $V_{i,j}(x)$.

We introduce a new potential that simulates the interaction of the atom with the α-particle, so the range of the function is of the order of the atomic radius.

$$V(x) = V_{1,2}(x) = V_{2,1}(x) = 2\lambda\beta^2 x e^{-\beta^2 x^2}, \quad \int_0^\infty V(x)dx = \lambda, \tag{4.4}$$

where as before λ and β are constants and $V_{i,i}(x) = 0$. We assume $\beta = 1$ throughout.

The exact form for the wavefunction of the system of the α-particle and the atom is written as

$$\Psi(x,t) = \phi_\alpha(x,t)[\chi_1(x,t)|1\rangle + \chi_2(x,t)|2\rangle], \tag{4.5}$$

where each state is assumed to have its own spatial dependence as well. In the Factorization Approximation the x-dependence of $\chi_i(x,t)$ is ignored.

$\phi_\alpha(x,t)$ is the solution of

$$\left(i\hbar\frac{\partial}{\partial t} - H_\alpha\right)\phi_\alpha(x,t) = 0. \tag{4.6}$$

We assume that (4.6) is solved and give an approximated heuristic form for it later.

Before proceeding further we look at the simpler classical approximation.

4.3 Migdal's Method for α-Decay

We now simulate the result for excitation probability by α decay proposed by Migdal (Migdal 1941) which was based on the classical trajectory of the α-particle, and is supported by experiment (Levinger 1953; Fischbeck and Freedman 1975;

Fischbeck and Freedman 1977). This model assumes a very simple form of the wavefunction for a 2-level atom in one dimension:

$$\Psi_{\rm M}(t) = c_1(t)|1\rangle + c_2(t)|2\rangle, \tag{4.7}$$

The particle is treated classically by having a set position and velocity at a given time, but the interaction with the atom is treated quantum mechanically with the time-dependent Schrödinger equation. The coefficients in (4.7) are found by solving

$$\left(i\frac{\partial}{\partial t} - \epsilon_i\right) c_i(t) = V(vt)c_j(t). \quad i \neq j. \tag{4.8}$$

where $V(x(t)) = V(vt) = 2\lambda vt\beta^2 e^{-(\beta vt)^2}$ and $x(t) = vt$ is the position of the point particle. As explained in KNvD, the potential enters the coupled equations in this way for the point particle because the interaction between the α-particle and the atomic electron is a δ-function potential.

Again we assume $c_{1,2}(t)$ is of the form: $c_{1,2}(t) = C_{1,2}(t)e^{-i\epsilon_{1,2}t}$ and the above coupled equations simplify to:

$$\frac{d}{dt}C_1(t) = -iV(vt)C_2(t)e^{i(\epsilon_1-\epsilon_2)t} \tag{4.9}$$

$$\frac{d}{dt}C_2(t) = -iV(vt)C_1(t)e^{i(\epsilon_2-\epsilon_1)t} \tag{4.10}$$

The initial condition is

$$c_1(0) = C_1(0) = 1, \quad c_2(0) = C_2(0) = 0. \tag{4.11}$$

The probability of transition from the first state to the second is the magnitude squared of the coefficient

$$P_{21}^M(t) = |c_2(t)|^2. \tag{4.12}$$

This result can also be obtained approximately for small values of the potential strength parameter λ, using perturbation theory.

Here we assume $c_1(t) = e^{-i\epsilon_1 t} \rightarrow C_1(t) = 1$. Then,

$$\begin{aligned} c_2(t) &= -ie^{-i\epsilon_2 t}\int_0^t V(vt')e^{i(\epsilon_2-\epsilon_1)t'}dt' \\ &= -ie^{-i\epsilon_2 t}(2\lambda\beta^2 v)\int_0^t t'e^{-(\beta vt')^2}e^{i(\epsilon_2-\epsilon_1)t'}dt' \end{aligned} \tag{4.13}$$

The coupled equations are solved for the initial condition using a variable step size Runge-Kutta integration method in Matlab, as in the previous chapter. The integral (4.13) in the perturbation method can be calculated numerically for a given t.

An example of the good agreement between these two methods, for increasing time, is shown in Figure 4.1. Perturbation theory is seen to work very well for $\lambda = 0.1$.

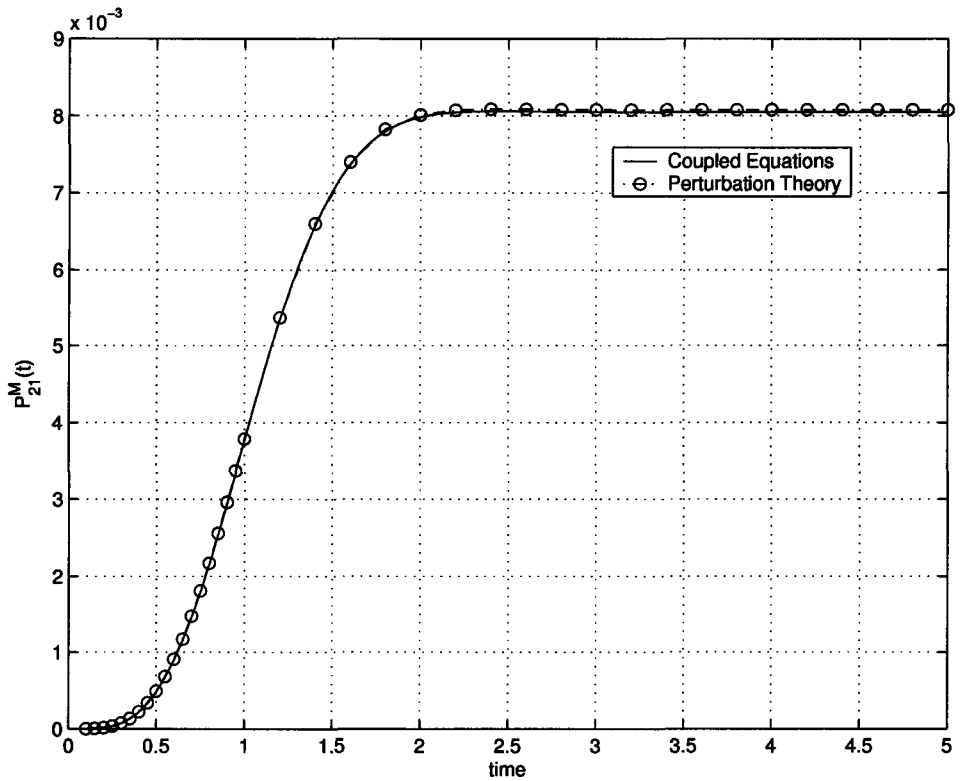

Figure 4.1: Simulation of Migdal's method: Comparison of transition probability using perturbation theory and solution of coupled equations for $\lambda = 0.1$, $v = \beta = 1$.

A comparison between the exact and perturbative solution to the coupled equations for increasing λ is shown in Figure 4.2. For λ equal to 1 and greater, the results diverge, but agree well for λ smaller than 1. It is important to know the appropriate values of λ for this new potential before calculating new results later in this chapter based on perturbation theory.

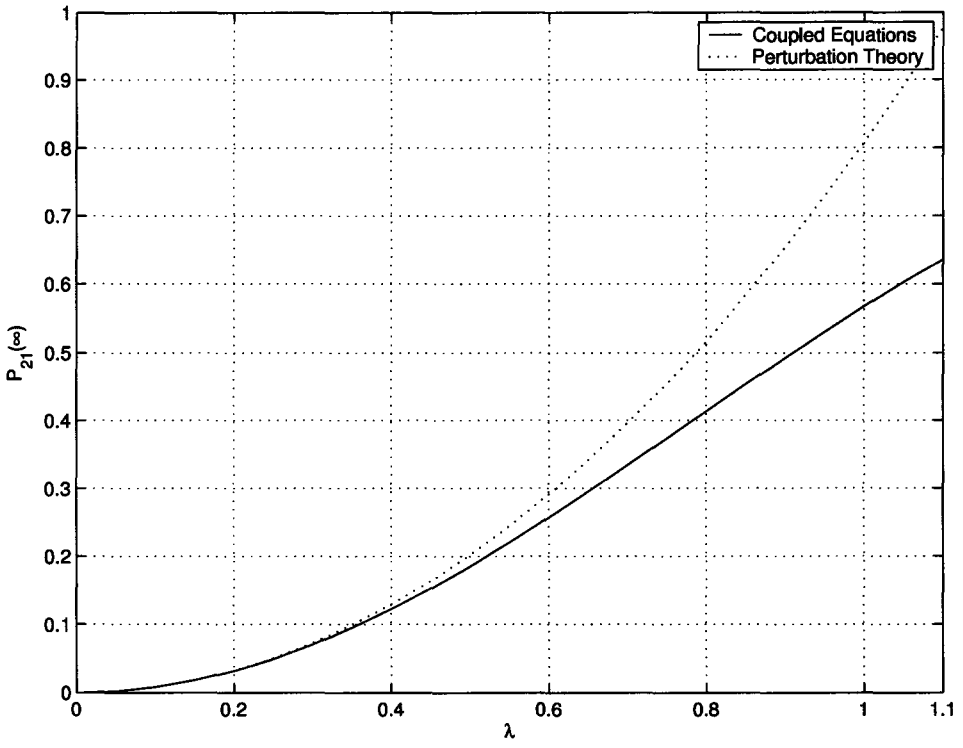

Figure 4.2: Migdal's method: Comparison of $P_{21}(\infty)$ using perturbation theory and solution of coupled equations, for varying potential strength λ with $v = \beta = 1$

4.4 Fully Quantum Mechanical Model

4.4.1 Structure of the Model

This model uses the general form of the wavefunction for the α-atom system with the heuristic form for the α-particle wavefunction proposed by Breit (Breit 1959) and van Dijk, et al. (van Dijk, Kataoka, and Nogami 1999), and the general form for the the states. This model corresponds closely to model IIb in KNvD as outlined earlier. No significant approximations are made until the end where the solution is obtained using perturbation theory. We begin by inserting

$$\Psi(x,t) = \phi_\alpha(x,t)[\chi_1(x,t)|1\rangle + \chi_2(x,t)|2\rangle], \tag{4.14}$$

into the wave equation (4.1)

$$\left(i\frac{\partial}{\partial t} - H\right)\Psi(x,t) = 0. \tag{4.15}$$

Recall that $H_\alpha\phi_\alpha(x,t)=i\frac{\partial}{\partial t}\phi_\alpha(x,t)$. This leads to the substitution

$$\begin{aligned} &H_\alpha\phi_\alpha(x,t)[\chi_1(x,t)|1\rangle + \chi_2(x,t)|2\rangle] = \\ &\left[\frac{p^2}{2m} + U_\alpha(x)\right]\phi_\alpha(x,t)[\chi_1(x,t)|1\rangle + \chi_2(x,t)|2\rangle]. \end{aligned} \tag{4.16}$$

Some cancellations can then be made and we arrive at the coupled equations for the χ's.

$$\left[i\frac{\partial}{\partial t} - \epsilon_i + \frac{1}{2m}\left(\frac{\partial^2}{\partial x^2} + F(x,t)\frac{\partial}{\partial x}\right)\right]\chi_i(x,t) = V(x)\chi_j(x,t), \tag{4.17}$$

where $i \neq j$ and

$$F(x,t) = \frac{2}{\phi_\alpha(x,t)}\frac{\partial\phi_\alpha(x,t)}{\partial x}. \tag{4.18}$$

It is now appropriate to give the assumed form of $\phi_\alpha(x,t)$. The exact solution to the Schrödinger equation for the α-particle (4.1) is generally highly complicated, but we assume it can be well approximated by the heuristic form. Its validity is confirmed by the exact form of the α-particle wavefunction of van Dijk and Nogami (van Dijk and Nogami 2002; van Dijk and Nogami 2004). The heuristic wavefunction is

$$\phi_\alpha(x,t) = \sqrt{\rho(x,t)}\exp\left\{-i\left[\omega - \frac{1}{2m}\left(\frac{\Gamma}{2v}\right)^2\right]t + ikx\right\}, \tag{4.19}$$

where

$$\begin{aligned}\rho_\alpha(x,t) &= |\phi_\alpha(x,t)|^2 \\ &= e^{-\Gamma t}\rho_\alpha(x,0) + \frac{\Gamma}{v}\exp\left[-\Gamma\left(t-\frac{x}{v}\right)\right]\theta\left(t-\frac{x}{v}\right),\end{aligned} \tag{4.20}$$

where $\theta(t)$ is a step function, equal to zero for $t<0$ and equal to one for $t>0$. At $t=0$, $\rho_\alpha(x,0)$ is confined to the nucleus, effectively between $x=0$ and $x=0^+$ on the atomic scale of this problem. The parameter Γ controls the width of the α wavefunction, and also defines the rate of decay of the α-particle from the nucleus. It is inversely proportional to the decay half-life: $\Gamma = (\ln 2)/\tau_{1/2}$.

Then, inserting (4.19) into (4.18) gives

$$\begin{aligned}F(x,t) &= i2k + \frac{1}{\rho_\alpha(x,t)}\frac{\partial}{\partial x}\rho_\alpha(x,t) = i2k + \frac{\partial}{\partial x}\ln\rho_\alpha(x,t) \\ &\cong i2k + \frac{\Gamma}{v} - \frac{\gamma}{v}f(-t+x/v),\end{aligned} \tag{4.21}$$

where we have approximated the step function $\theta(x)$ in $\rho_\alpha(x,t)$ by the function $f(x) = 1/(1+e^{-\gamma x})$, with γ chosen so that the step function is steep on the scale of the problem. The second line in (4.21) uses the fact that $f^{-1}(x)df(x)/dx = \gamma f(-x)$.

Equation (4.17) for $\chi_{i,j}(x,t)$ is similar to the non-homogeneous coupled Schrödinger equation discussed in chapter 2 with the exception of the first derivative term in x. We need to remove this term before proceeding. Begin by rewriting $\chi_i(x,t)$ as

$$\chi_i(x,t) = \xi_i(x,t) \exp\left[-\frac{1}{2}\int_{0^+}^{x} F(x,t)dx\right]. \tag{4.22}$$

The lower limit of $x = 0^+$ is arbitrary, but was chosen in this way so that the $\rho_\alpha(x,0)$ terms in (4.20) can be ignored when calculating the integral.

Substituting $\chi_i(x,t)$ into (4.17) leads to first derivative terms in $\chi_i(x,t)$, but these cancel out after the first step. Then the exponential of the integral cancels out of all the terms but the time derivative one and we are left with

$$\left[i\frac{\partial}{\partial t} - \epsilon_i + \frac{1}{2m}\frac{\partial^2}{\partial x^2} - G(x,t)\right]\xi_i(x,t) = V(x)\xi_j(x,t), \tag{4.23}$$

where

$$G(x,t) = \frac{1}{4m}\frac{\partial F(x,t)}{\partial x} + \frac{1}{8m}F^2(x,t) + \frac{i}{2}\frac{\partial}{\partial t}\left(\int_{0^+}^{x} F(x,t)dx\right) \tag{4.24}$$

The function $G(x,t)$ acts as a time-dependent potential that restrains the extent of the wavefunction. It is essentially an expanding well that moves out from the origin at velocity $v = 1$.

The transition probability for this model is

$$\begin{aligned}
P_{21}^{\alpha}(t) &= \int_0^\infty |\chi_2(x,t)|^2 \rho_\alpha(x,t)dx && (4.25)\\
&= \int_0^\infty \left|\xi_2(x,t)\exp\left[-\frac{1}{2}\int_{0^+}^{x} F(x,t)dx\right]\right|^2 \rho_\alpha(x,t)dx && (4.26)\\
&= \int_0^\infty \left|\xi_2(x,t)e^{-ikx}\sqrt{\frac{\rho_\alpha(0^+,t)}{\rho_\alpha(x,t)}}\right|^2 \rho_\alpha(x,t)dx && (4.27)\\
&= \rho_\alpha(0^+,t)\int_0^\infty |\xi_2(x,t)|^2 dx. && (4.28)
\end{aligned}$$

In (4.25), we used that

$$\int_{0+}^{x} F(x,t)dx = 2ikx + \ln\left(\frac{\rho_\alpha(x,t)}{\rho_\alpha(0^+,t)}\right). \tag{4.29}$$

4.4.2 Perturbation Theory

Equation (4.23) is simpler than the corresponding equation in KNvD. This removes some of the difficulty of that work so we have succeeded in that regard, but it is still complicated to solve, so we again turn to perturbation theory. Assume that

$$\chi_1(x,t) = e^{-i\epsilon_1 t}, \quad \chi_2(x,t) = 0. \tag{4.30}$$

Then

$$\xi_1(x,t) = e^{-i\epsilon_1 t}\exp\left[\frac{1}{2}\int_{0+}^{x} F(x,t)dx\right], \quad \xi_2(x,t) = 0, \tag{4.31}$$

and (4.23) becomes

$$\left[i\frac{\partial}{\partial t} - \epsilon_2 + \frac{1}{2m}\frac{\partial^2}{\partial x^2} - G(x,t)\right]\xi_2(x,t) = V(x)e^{-i\epsilon_1 t}\exp\left[\frac{1}{2}\int_{0+}^{x} F(x,t)dx\right]. \tag{4.32}$$

Comparing with the general form of the non-homogeneous equation (2.7) shows that

$$\begin{aligned} U(x,t) &= \epsilon_2 + G(x,t) \\ N(x,t) &= V(x)e^{-i\epsilon_1 t}\exp\left[\frac{1}{2}\int_{0+}^{x} F(x,t)dx\right] \end{aligned}$$

The model can thus be solved with the non-homogeneous formulation put forth in chapter 2.

An example of a comparison between this model and the much more simplistic classical approach (from the previous section) is shown in Figure 4.3. We see excellent agreement between the two approaches for for $t \rightarrow \infty$, for a range of the wavefunction width parameter, Γ. At $t = \infty$ the agreement is about 1.5%. This is in contrast to the KNvD result that showed two to six orders of magnitude discrepancy between the two approaches.

The result for $t \rightarrow \infty$ is shown to be independent of the decay rate Γ, similar to the result of van Dijk, et al. (van Dijk, Kiers, Nogami, Platt, and Spyksma 2003), and our chapter 3, for the more schematic model. For early times there is large variation in the transition, with transitions occurring much slower for small Γ as one would expect as a large portion of the wavefunction still resides in the nucleus. As Γ increases, the time dependent behaviour becomes closer to the classical result. This can be seen as the α particle wavefunction approaching a δ-function, representative of a point particle. We note as an aside that in KNvD, equation (2.12) takes into account that, although it is assumed that the alpha particle is emitted at $t = 0$ in the classical approximation, we actually do not now when the emission takes place. We only know the probability for the emission in the time interval of t and $t + \Delta t$, which is $\Gamma e^{\gamma t} \Delta t$. If we use KNvDs (2.12), we will find better time-dependent agreement

The results are converged on this scale for the spatial and temporal mesh sizes of $h = \Delta t = 0.002$ with very minor changes when $h = \Delta t = 0.001$. The choice of $\gamma = 100$ used in the simulation of the step function was also found to be appropriate as no change was visible after changing the parameter to $\gamma = 50$.

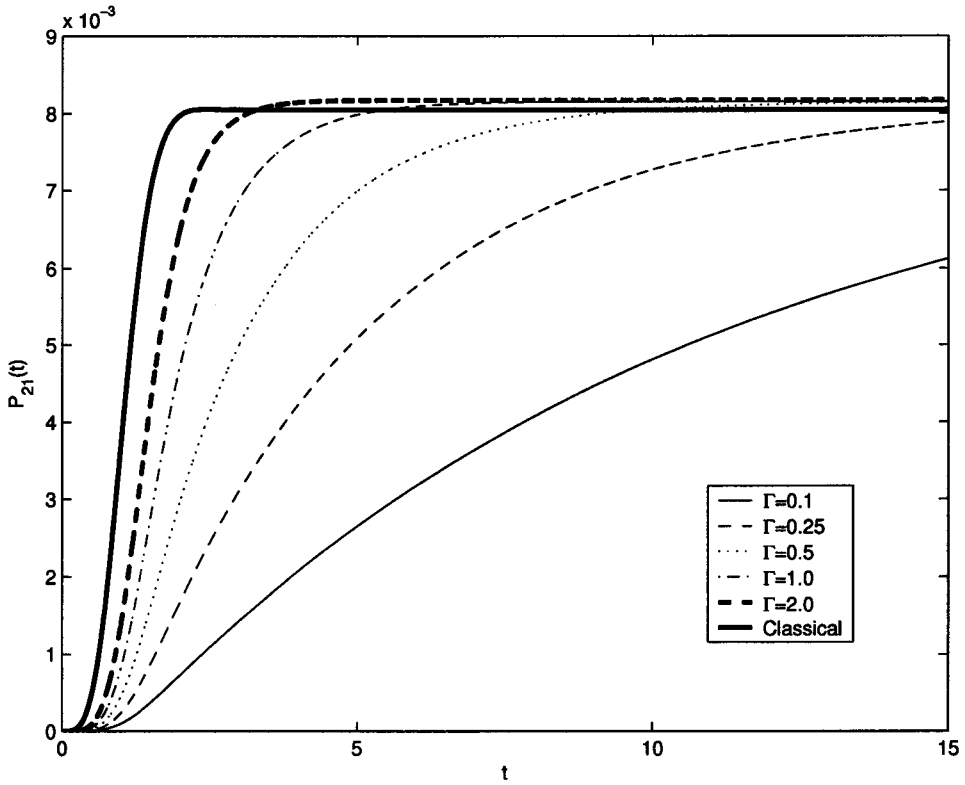

Figure 4.3: Comparison of fully quantum mechanical approach using perturbation theory with classical approach. $v = 1$. At $t = \infty$ the asymptotic values of $P_{21}(t)$ for the two methods agree to about 1.5%.

Figure 4.4 shows $|\xi_2(x,t)|^2$ propagating in time, for the case where $\lambda = 0.1$, $\Gamma = 0.25$, $v = \beta = 1$. The effect of the $G(x,t)$ function to hold the wavefunction within a defined region is clearly seen. The wavefunction appearance was also not affected by reducing the mesh size or decreasing the γ parameter. The ripple in the wavefunction appears to be the wave interfering with itself within the $G(x,t)$ imposed potential.

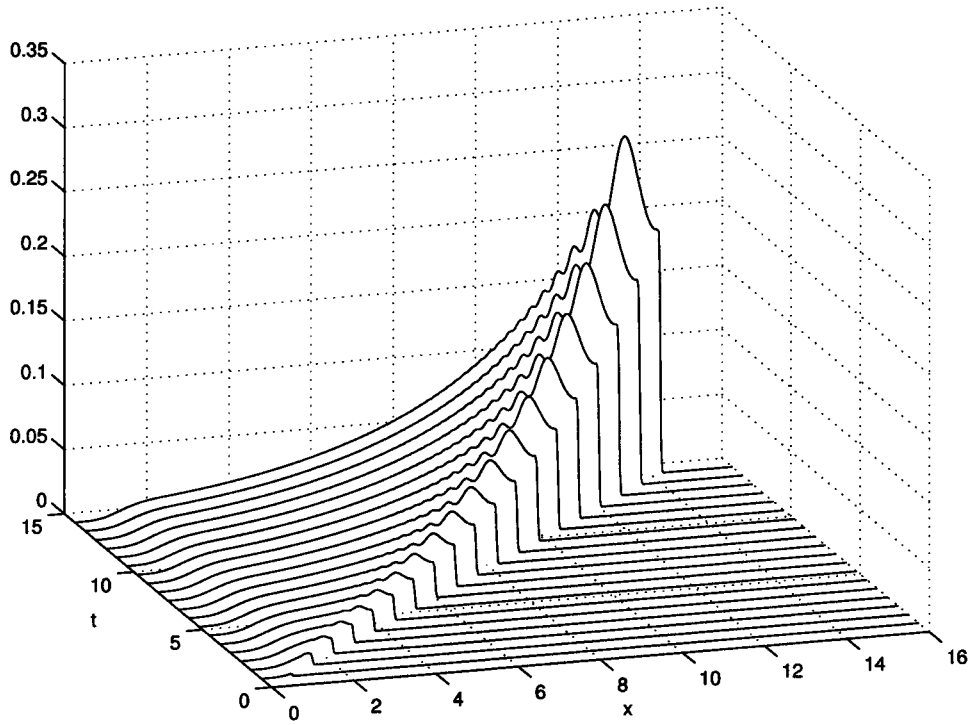

Figure 4.4: $|\xi_2(x,t)|^2$ for $\lambda = 0.1$, $\Gamma = 0.25$.

Figure 4.5 shows the magnitude squared of the state $\chi_2(x,t)$. In approximation A in the previous chapter and in the Factorization approximation in the next section we assume that the $\chi_i(x,t)$ is independent of x, but it is clear that this is not the case. Although it is approximately constant for a region of x, there is a large x dependency near the origin $x = 0$, and near the wavefront at $x = vt$

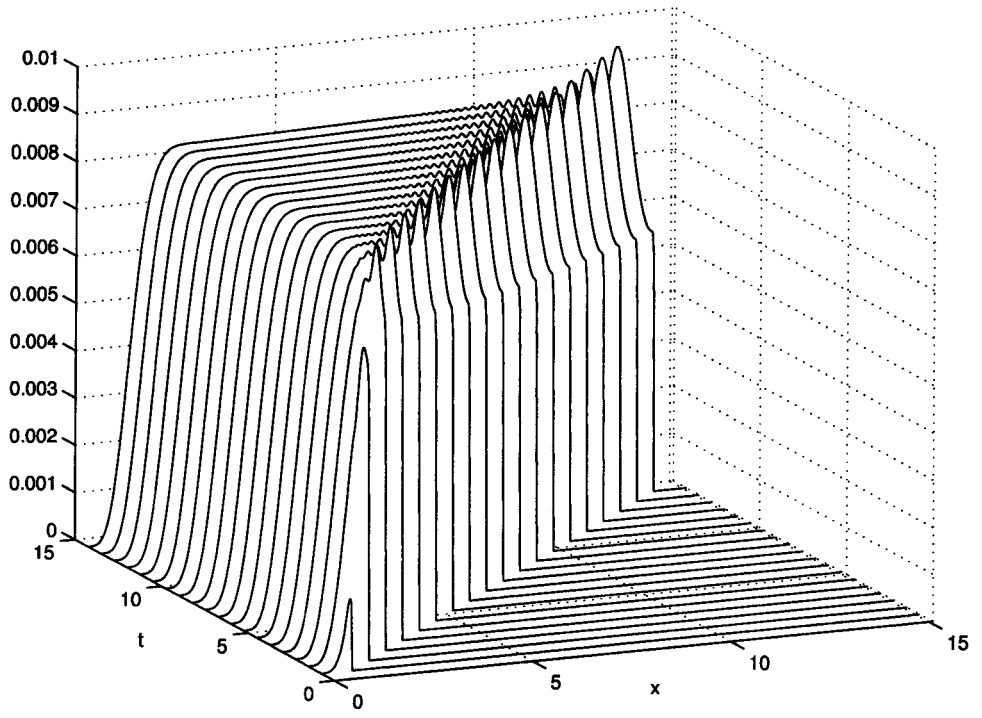

Figure 4.5: $|\chi_2(x,t)|^2$ for $\lambda = 0.1$, $\Gamma = 0.25$.

The magnitude squared of the corresponding wavefunction for this state $|\Psi_2(x,t)|^2 = |\phi_\alpha(x,t)\chi_2(x,t)|^2$ is seen in Figure 4.6. We see that the peak is approached rapidly in time and then remains constant. The integral of this plot (the transition probability) continues to grow until the α-particle wavefunction has left the nucleus.

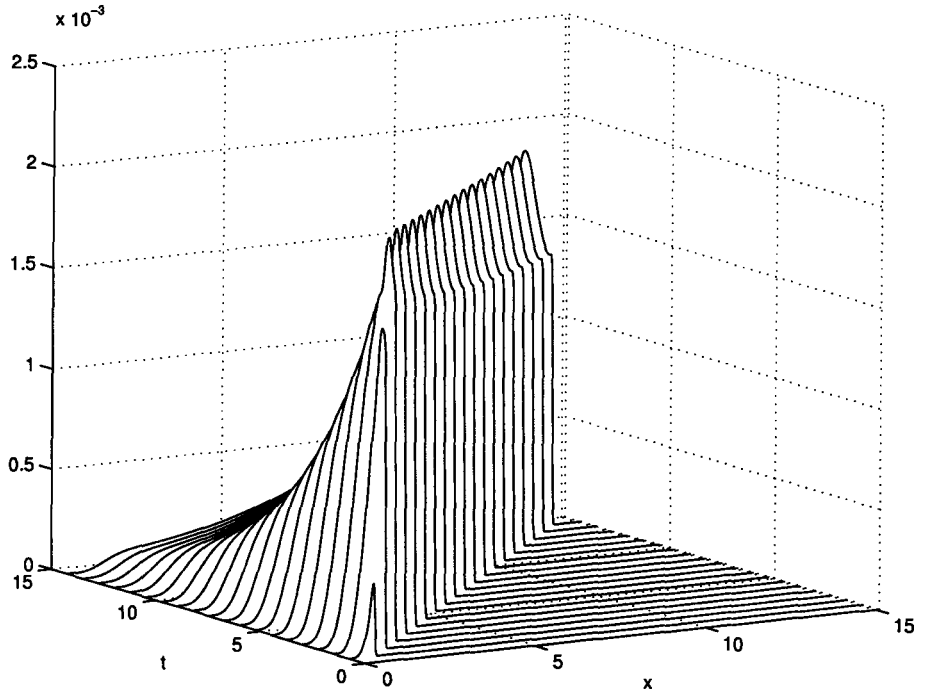

Figure 4.6: $|\Psi_2(x,t)|^2 = |\phi_\alpha(x,t)\chi_2(x,t)|^2$ for $\lambda = 0.1$, $\Gamma = 0.25$.

4.5 Factorization Approximation

For this approximation we assume that the χ_i are independent of x as in Approximation A in chapter 3. This model corresponds to model IIa of KNvD, making the assumption that $\phi_\alpha(x,t)$ is not affected by interactions with the atom. We assume

$$\Psi_F(x,t) = \phi_\alpha(x,t)[\chi_1(t)|1\rangle + \chi_2(t)|2\rangle]. \tag{4.33}$$

As in chapter 3, Approximation A, this form for the wavefunction leads to the coupled equations

$$\left(i\frac{d}{dt} - \epsilon_i\right)\chi_i(t) = W_F(t)\chi_j(t), \quad i \neq j, \tag{4.34}$$

where

$$W_F(t) = \int_0^\infty \rho_\alpha(x,t)V(x)dx. \tag{4.35}$$

As in the previous section

$$\rho_\alpha(x,t) = e^{-\Gamma t}\rho_\alpha(x,0) + \frac{\Gamma}{v}\exp\left[-\Gamma\left(t-\frac{x}{v}\right)\right]\theta\left(t-\frac{x}{v}\right), \tag{4.36}$$

and

$$V(x) = 2\lambda\beta^2 x e^{-\beta^2x^2}. \tag{4.37}$$

$W_F(t)$ can be worked out explicitly as

$$\begin{aligned} W_F(t) &= -\frac{\lambda\Gamma}{v}e^{-\Gamma t}\int_0^{vt} e^{\Gamma x/v}\frac{d}{dx}e^{-\beta^2x^2}dx \\ &= \frac{\lambda\Gamma}{v}\left[e^{-\Gamma t} - e^{-(\beta vt)^2} + \frac{\Gamma}{v}e^{-\Gamma t}\int_0^{vt} e^{\Gamma x/v}e^{-\beta^2x^2}dx\right]. \end{aligned} \tag{4.38}$$

The last integral is

$$\begin{aligned}\int_0^{vt} e^{\Gamma x/v} e^{-\beta^2 x^2} dx &= e^{(\Gamma/2\beta v)^2} \int_0^{vt} \exp\left[-\left(\beta x - \frac{\Gamma}{2\beta v}\right)^2\right] dx \\ &= e^{(\Gamma/2\beta v)^2} \frac{\sqrt{\pi}}{2\beta}\left[\mathrm{erf}\left(\beta vt - \frac{\Gamma}{2\beta v}\right) + \mathrm{erf}\left(\frac{\Gamma}{2\beta v}\right)\right] \quad (4.39)\end{aligned}$$

where the error function $\mathrm{erf}(z) = (2/\sqrt{\pi}) \int_0^z e^{-y^2} dy$.

For the coupled equation solution we use the initial condition

$$\chi_1(0) = 1, \quad \chi_2(0) = 0. \quad (4.40)$$

The probability for transition $1 \rightarrow 2$ in this approximation is given by

$$P_{21}^F(t) = |\chi_2(t)|^2. \quad (4.41)$$

Before looking at results we will again apply perturbation theory to the problem. In this case set $\chi_1(x,t) = e^{-i\epsilon_1 t}$ and insert into (4.34) with $i = 2$ and $j = 1$. The coefficient for the excited state is then

$$\chi_2(t) = -ie^{-i\epsilon_2 t} \int_0^t W(t') e^{i(\epsilon_2 - \epsilon_1)t'} dt', \quad (4.42)$$

and

$$P_{21}^{F,PT}(t) = |\chi_2(t)|^2 \quad (4.43)$$

as before.

We can gain some insight into the forthcoming results by looking at an approximate version of $W_F(t)$ that leads to an analytic form for the transition probability from perturbation theory (an analytic result is also possible for $\chi_1(t)$ and $\chi_2(t)$,

although not shown here, if this $W_F^{approx}(t)$ is substituted into the coupled equations). $W_F(t)$ quickly peaks with increasing t, and has an exponential tail which can be well approximated by

$$W_F^{approx}(t) = \lambda\Gamma e^{-\Gamma(t-t_0)}\theta(t-t_0). \tag{4.44}$$

The peak of the potential $V(x)$ from (4.37) is at $x = 1/(\beta\sqrt{2})$ and the front peak of the wavepacket (4.36) moves at a velocity v so set the edge t_0 of $W_F^{approx}(t)$ to $t_0 = 1/(v\beta\sqrt{2})$ so that $W_F^{approx}(t)$ mimics the shape of $W_F(t)$. Figure 4.7 shows the $W_F(t)$ and $W_F^{approx}(t)$ plotted versus time for $\lambda = \Gamma = 0.1$, $\Delta\epsilon = \epsilon_2 - \epsilon_1 = 1 - 0 = 1$, and $\beta = v = 1$. We see excellent agreement between the two in the tail region. The approximate version of $W_F(t)$ can also be used in the coupled equation formulation of this problem (4.34).

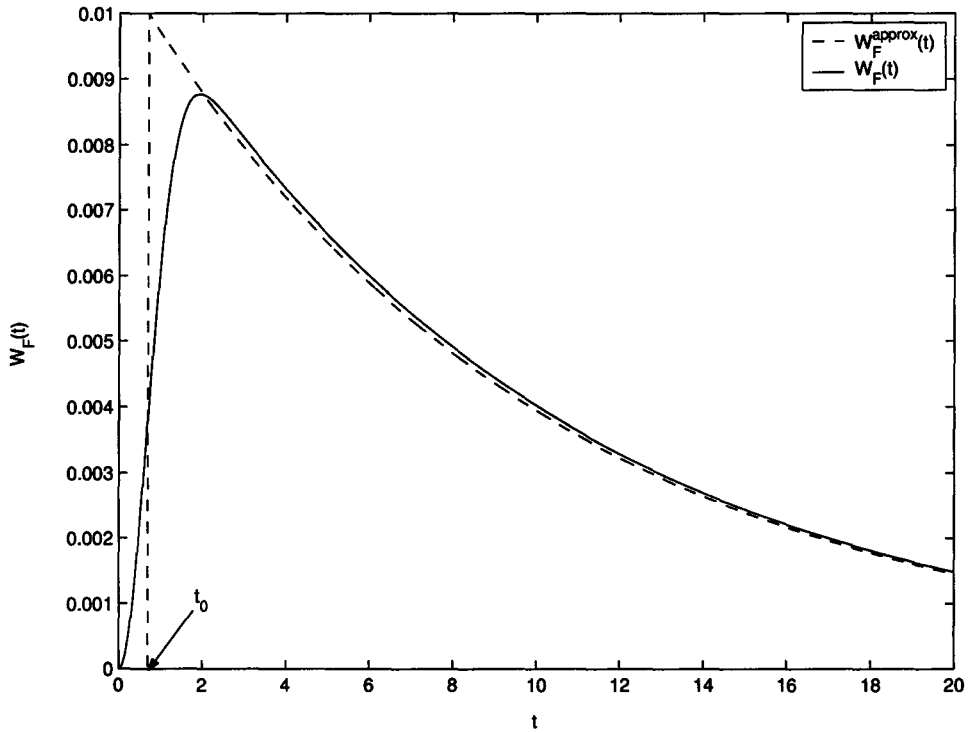

Figure 4.7: A comparison between $W_F(t)$ and $W_F^{approx}(t)$. $\lambda = \Gamma = 0.1$, $\Delta\epsilon = \epsilon_2 - \epsilon_1 = 1 - 0 = 1$, and $\beta = v = 1$.

Inserting (4.44)into (4.42) gives

$$\begin{aligned}\chi_2(t) &= -ie^{-i\epsilon_2 t}\int_0^t W(t')e^{i\Delta\epsilon t'}dt' \\ &\approx -ie^{-i\epsilon_2 t}\lambda\Gamma\theta(t-t_0)\int_{t_0}^t e^{-\Gamma(t'-t_0)e^{i\Delta\epsilon t'}}dt' \\ &= -ie^{-i\epsilon_2 t}\frac{\lambda\Gamma e^{i\Delta\epsilon t_0}}{\Gamma - i\Delta\epsilon}\left[1-e^{-(\Gamma-i\Delta\epsilon)(t-t_0)}\right]\theta(t-t_0). \qquad (4.45)\end{aligned}$$

Then the transition probability is

$$P_{21}^{F,approx}(t) = \frac{(\lambda\Gamma)^2}{\Gamma^2+(\Delta\epsilon)^2}\left[1+e^{-2\Gamma(t-t_0)}-2e^{-\Gamma(t-t_0)}\cos(\Delta\epsilon(t-t_0))\right]\theta(t-t_0). \qquad (4.46)$$

As $t \to \infty$ the exponential terms in t die off and the transition probability is approximately found from

$$P_{21}^{F,approx}(t=\infty) = \frac{(\lambda\Gamma)^2}{\Gamma^2+(\Delta\epsilon)^2}. \qquad (4.47)$$

We now look at some results of these approximations. In these models, the strength of the potential is governed by the parameter λ. Since we will be applying perturbation theory it is appropriate to examine the values of λ expected to give good results. Figure 4.8 shows the results of the coupled equations (4.34) with $W_F(t)$ versus the perturbation result (4.43) for the same $W_F(t)$. For $\lambda < 1$ there is excellent agreement while for $\lambda \approx 5$ the difference is almost 100%.

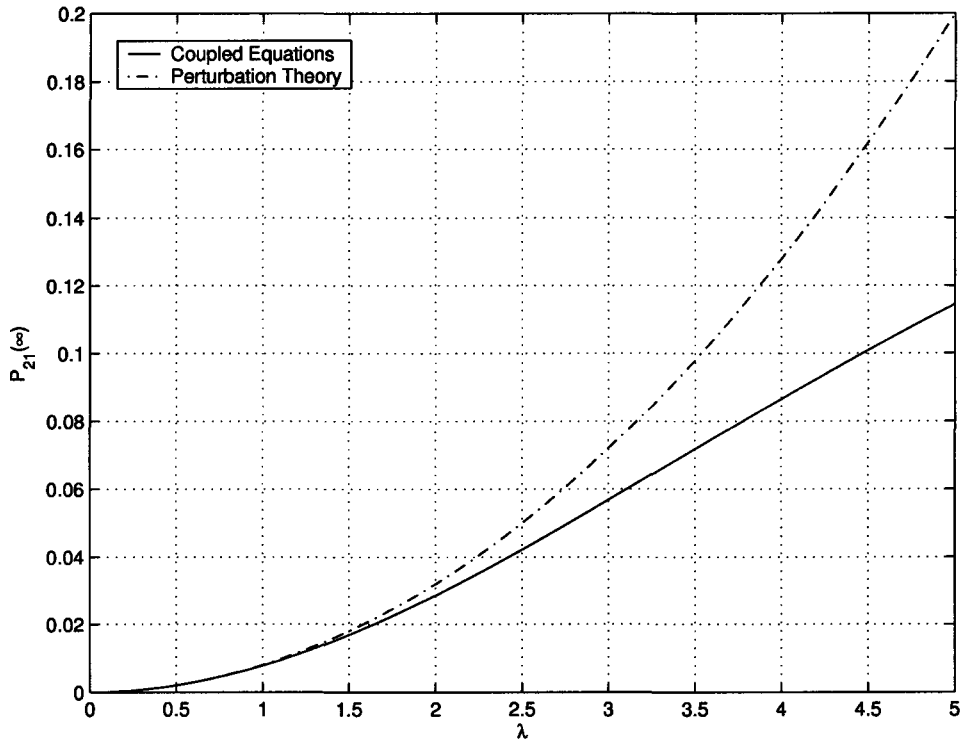

Figure 4.8: A comparison the CE solution and the perturbation approximation, using $W_F(t)$, for varying potential strength λ.

We now look at results for the transition probability predicted by the factorization approximation from the four versions of the model we have been discussing: (1) coupled equation solution (4.34) with $W_F(t)$, (2) coupled equation solution (4.34) with $W_F^{approx}(t)$, (3) perturbation theory (4.43) with $W_F(t)$, and (4) perturbation theory (4.43) with $W_F^{approx}(t)$. We use $\lambda = \Gamma = 0.1$, $\Delta\epsilon = \epsilon_2 - \epsilon_1 = 1 - 0 = 1$, and $\beta = v = 1$.

The results are summarized in Figure 4.9. The oscillations die out quickly and are essentially indiscernible on this scale after $t \approx 75$, at which point the two curves for $W_F^{approx}(t)$ converge to $P_{21}^{F,approx}(t = \infty) = 9.9 \times 10^{-5}$ as suggested by (4.47), for the values used. Perturbation theory works well for this value of λ as the two curves (solid and dashed) for $W_F(t)$ overlap almost perfectly. Perturbation theory works well for the approximate $W_F^{approx}(t)$ also. From the results in Figure 4.8 this agreement is expected for $\lambda = 0.1$.

There is a small difference between the approximate and exact versions of $W_F(t)$ with the transition probability being higher in the case of the approximate version. This possibly due to the higher peak in $W_F^{approx}(t)$, as seen in Figure 4.7. This higher peak mimics a slightly higher peak overlap between $\rho_\alpha(x,t)$ and $V(x)$ in (4.35).

The period of oscillations can be predicted from (4.46) where the harmonic cos() term contains the argument $\Delta\epsilon(t - t_0)$ leading to a period $T = 2\pi/\Delta\epsilon = 2\pi$, as seen in the figure.

A comparison of the factorization approximation with the classical result using Migdal's method, which gives $P_{21}(\infty) \approx 0.008$, as shown in Figure 4.3, shows a large difference between the predicted transition probabilities of the two methods. Note that although Figure 4.3 uses $\Gamma = 0.5$, the Γ parameter does not appear in

the formulation for the classical result. The results here and in Approximation A in chapter 3 are both in disagreement with the classical result. The factorization approximation is clearly not a valid approach to calculating transition probabilities as the predictions are about two orders of magnitude different.

This approximation also assumes that $\chi_2(x,t)$ is constant in x, but as we saw in the last section in Figure 4.5, $\chi_2(x,t)$ does alter $\phi_\alpha(x,t)$ so there is a spatial dependence to $\chi_2(x,t)$.

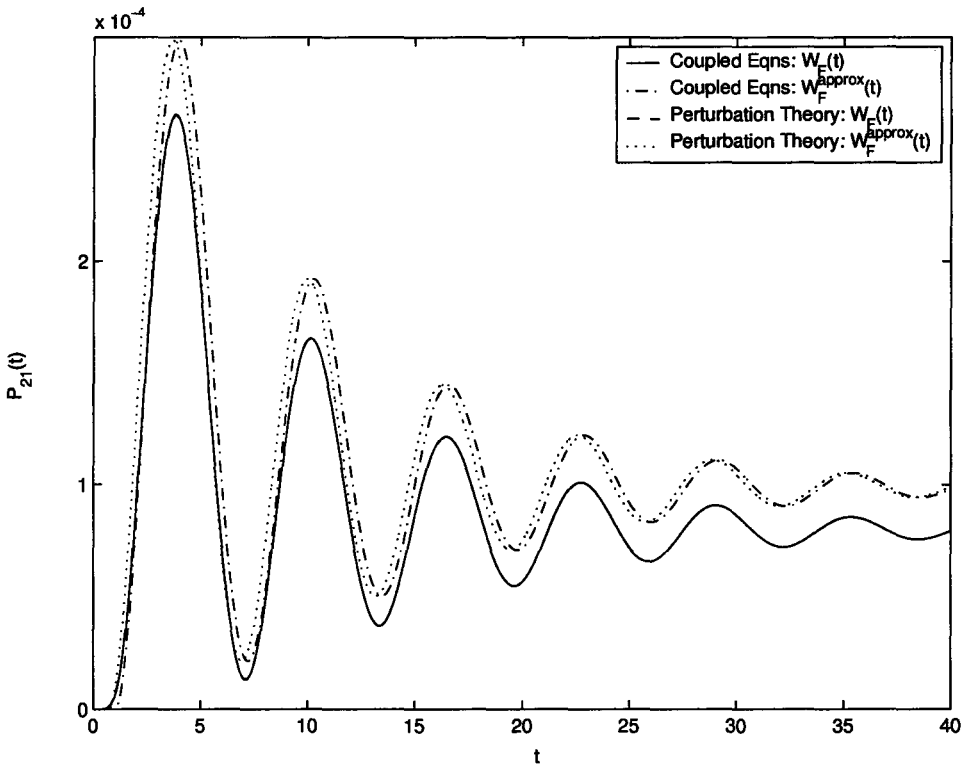

Figure 4.9: A comparison between the coupled equation solution and perturbation theory for two versions of $W_F(t)$ for the factorization approximation with $\lambda = \Gamma = 0.1$, $\Delta\epsilon = \epsilon_2 - \epsilon_1 = 1 - 0 = 1$, and $\beta = v = 1$.

4.6 Relation with KNvD's calculations

Since it appears in this work that there is agreement between the exact model, or at least the first order PT approximation of the exact treatment of the problem, with the classical result simulating Migdal's method it is important to look more closely at the model of KNvD to see if the source of the discrepancy is apparent. Recall that KNvD predicted approximate agreement between their models IIa and IIb, but that the difference between these two models and their model I, corresponding to the classical point particle, was several orders of magnitude, depending on the interaction strength.

It is clear from our work in chapters 3 and 4 that a large difference should be expected between the Factorization approximation where $\Psi(x,t)$ is of the form

$$\Psi_F(x,t) = \phi_\alpha(x,t)[\chi_1(t)|1\rangle + \chi_2(t)|2\rangle], \tag{4.48}$$

and the classical result. In our schematic model of chapter 3 and the more physical model of chapter 4, a significant difference was seen in the predicted excitation probabilities arising from this approximation. In this sense we agree with the KNvD result for their model IIa. This is still somewhat surprising since changes to the α-particle wavefunction are expected to be minimal in this interaction.

We speculate that the problem is in KNvD model IIb. In this model they use a Pöschl-Teller potential which is proportional to $1/\cosh^2(\lambda_e x_e)$ where $1/\lambda_e$ is the atomic radius and x_e is the coordinate of the electron. KNvD chose the electron bound states such that their wavefunctions vanish at the origin. KNvD assumed a contact interaction between the electron and the α-particle and the effective potential between the atom and the α-particle that follow from this vanishes at the origin. This aspect is well simulated by our $V(x)$ that vanishes at the origin. They chose the potential strength such that there were only two bound states.

There is also the probability that state 1 is excited into an unbound or scattering state and this is accounted for in their model.

The wavefunction at a given time then is a combination of these states as prescribed by the coefficients C_n and C_ϵ.

$$\psi(x_e, x, t) = \sum_{n=1,3} C_n(x,t)\chi_n(x_e)e^{-i\epsilon_n t} + \int_0^\infty d\epsilon C_\epsilon(x,t)\chi_\epsilon(x_e)e^{-i\epsilon t}, \qquad (4.49)$$

where $\chi_n(x_e)$, for example, is the time-independent (real) wave function of the atomic state n with energy ϵ_n and x_e is the coordinate of the electron.

Using first order PT, this leads to an equation for the coefficients similar to our (4.23)

$$\left[i\frac{\partial}{\partial t} - \epsilon_n + \frac{1}{2m}\left(\frac{\partial^2}{\partial x^2} + F(x,t)\frac{\partial}{\partial x}\right)\right] C_n(x,t)$$
$$= -g\chi_n(x)\sum_{n'}\chi_{n'}(x)e^{i(\epsilon_n - \epsilon_{n'})t}C_{n'}(x,t), \qquad (4.50)$$

where g is the strength of the $\delta(x_e - x)$-function interaction between the α-particle and the electron interaction.

To recover our fully QM model from the KNvD we begin by dropping the integral term for the wavefunction in (4.49) thereby ignoring coupling to scattering states. If we also take only the part of the interaction that couples states $n = 1$ and $n = 3$, (4.50) is reduced to the form of our coupled equation for the problem (4.23), with $V(x) = -g\chi_1(x)\chi_3(x)$ except that there are "diagonal" terms with $n = n'$ and $\epsilon = \epsilon'$. Ignoring the diagonal term with $n = n'$ and further assuming that $g\chi_1^2(x) = g\chi_3^2(x) = V(x)$, then KNvD's model is reduced to the one we are using in this work. Although the diagonal terms are larger in magnitude than the off-diagonal terms of $n \neq n'$, the transition of state 1 to state 3, is directly caused by the off-diagonal interaction while the diagonal terms have only indirect,

or second-order effects. Our model clearly captures the main physics of model IIb, and the results should correspond. KNvD claim that their model IIb was more difficult to solve than model IIa and that instabilities were encountered in solving the problem for large time. This may be a symptom of problems for earlier times as well and the agreement between their models IIa and IIb may have masked this problem. This agreement does not seem to be coincidental though as it was seen for two very different interaction strengths. Considering the drastic effect of the factorization approximation on the result, where this approximation was thought to be minor, it is still possible that some of these subtle differences between our fully QM model and KNvD model IIb will still cause a large discrepancy. At this time the real cause for the difference is still unclear.

Chapter 5

Conclusions

5.1 Summary

In conclusion we have extended a powerful numerical method capable of solving the Schrödinger wave equation and have reformulated it so that it can solve N-channel interaction type problems. The method is fast, accurate and efficient and can operate on a standard desktop computer. The method has also been extended to be able to solve a special class of 1-channel non-homogeneous wave equations that arise in interaction problems when perturbation theory is applied to the coupled equations.

This model was then used to investigate some approximations that are made when modelling nuclear decay due to quantum particle interactions. We looked carefully at the approximation to the α-atom wavefunction where the α particle wavefunction is assumed to be unaffected by the interaction with the atom and found that in both cases (Approximation A in chapter 3, and the Factorization Approximation in chapter 4) that the results are not as expected based on the classical theory and experiment. It has become clear that this approximation to the wavefunction, though apparently mild, is invalid. For this reason it is not surprising that the results of KNvD for a similar model also do not correspond to the classical result.

We have also closely investigated a fully QM model of the interaction between a decaying particle (in this case an α-particle) and an atom. In this model we assume the general form of the α-atom wavefunction. Our solution to the problem was found to agree with the classical model, and hence with experiment. It was also found, similar to the schematic treatment by van Dijk, et al. (van Dijk, Kiers, Nogami, Platt, and Spyksma 2003), that the probability of transition after a long time is the same regardless of the decay rate of the α-particle, as we would expect classically. In a sense this is similar to the idea of flipping a coin now and again tomorrow; one week from now the probability of having heads will be the same. The α-particle classically has to leave the nucleus sometime and when it does the probability of excitation in the long run should be the same. It seems then that it is possible to properly model this quantum phenomenon. Some question still remains about what went wrong in model IIb of KNvD.

5.2 Suggestions for Future Work

This work is ongoing, but since the model has been shown to work it would be useful to apply this model to the β-decay problem. This problem has also been treated by Migdal. That is, the β-particle is treated as a classical particle. If the β-decay process is very slow in the atomic scale, which is usually the case, a problem very similar to what we have discussed in this thesis again arises. An important difference between the α and β cases is the β-particle (i.e., electron) is very light and its energy is large, typically of the order of a few MeVs.

Another outstanding problem is the exact (numerical) solution to the coupled equations arising from the fully QM model (4.23). We have successfully treated this equation with perturbation theory, but have not found results that com-

pletely agree when trying to solve the coupled equations. I believe there is some subtlety in the initial conditions and the other parameters that is suppressed in the perturbative solution.

The model presented here can be improved incrementally in sophistication bringing it closer to the KNvD model. This may uncover some assumption where their model IIb breaks down.

Bibliography

Breit, G. 1959. *Encyclopedia of Physics Vol. 41.* Springer, Berlin.

Fischbeck, H. J. & Freedman, M. S. 1975, Phys. Rev. Lett. *34*(4), 173–176.

Fischbeck, H. J. & Freedman, M. S. 1977, Phys. Rev. A *15*(1), 162–171.

Flügge, S. 1974. *Practical Quantum Mechanics.* Springer, Berlin.

Goldberg, A., Schey, H. M., & Schwartz, J. L. 1967, Am. J. Phys. *35*(3), 177–186.

Griffiths, D. J. 1995. *Introduction to Quantum Mechanics.* Prentice Hall, New Jersey.

Kataoka, F. 1998. Master's thesis, McMaster University, Hamilton.

Kataoka, F., Nogami, Y., & van Dijk, W. 2000, J. Phys. A: Math. Gen., 33, 5547–5566.

Leforestier, C. 1991, J. Comput. Phys., 94, 59–80.

Levinger, J. S. 1953, Phys. Rev. *90*(1), 11–25.

Liboff, R. L. 1991. *Introductory Quantum Mechanics* (2nd ed.). Addison-Wesley, Reading.

Migdal, A. 1941, J. Phys. (USSR) *4*(5), 449–453.

Moyer, C. A. 2003, Am. J. Phys *72*(3), 351–358.

Nogami, Y. & van Dijk, W. 2001, Few-Body Systems Suppl., 13, 196–205.

Pöschl, G. & Teller, F. 1933, Z. Phys., 83, 143–151.

Puzyin, I., Selin, A., & Vinitsky, S. 2000, Comput. Phys. Comm., 126, 158–161.

Tal-Ezer, H. & Kosloff, R. 1984, J. Chem. Phys., 81, 3967–3971.

van Dijk, W., Kataoka, F., & Nogami, Y. 1999, J. Phys. A: Math. Gen., 32, 6347–6360.

van Dijk, W., Kiers, K. A., Nogami, Y., Platt, A., & Spyksma, K. 2003, J. Phys. A: Math. Gen., 36, 5625–5643.

van Dijk, W. & Nogami, Y. 1999, Phys. Rev. Lett. *83*(15), 2867–2871.

van Dijk, W. & Nogami, Y. 2002, Phys. Rev. C *65*(024608), 1–14.

van Dijk, W. & Nogami, Y. 2004, Phys. Rev. C *70*(039901(E)), 1–1.